255700-4-F
Final Report

MULTI-APERTURE SYNTHESIS RADAR COMPARISON STUDY

H. KLIMACH

Environmental Research Institute of Michigan
P.O. Box 134001
Ann Arbor, MI 48113-4001

FEBRUARY 1995

Prepared For:

Army Research Laboratories
ATTN: AMSRL-SS-SC
2800 Powder Mill Rd.
Adelphi, MD 20783-1197

19960201 022

DTIC QUALITY INSPECTED 8

Contract Number: DAAL01-93-C-0074

ERIM-320

REPORT DOCUMENTATION PAGE

Form Approved
OMB No. 0704-0188

Public reporting burden for the collection of information is estimated to average 1 hour per response, including the time for reviewing instructions, searching existing data sources, gathering and maintaining the data needed, and completing and reviewing the collection of information. Send comments regarding this burden estimate or any other aspect of this collection of information, including suggestions for reducing this burden, to Washington Headquarters Services, Directorate for Information Operations and Reports, 1215 Jefferson Davis Highway, Suite 1204, Arlington, VA 22202-4302, and to the Office of Management and Budget, Paperwork Reduction Project (0704-0188), Washington, DC 20503.

1. AGENCY USE ONLY (*Leave Blank*)	2. REPORT DATE February 1995	3. REPORT TYPE AND DATES COVERED August 1993 – February 1995

4. TITLE AND SUBTITLE
Multi-Aperture Synthesis Radar Comparative Study

5. FUNDING NUMBERS

6. AUTHOR(S)
H. Klimach

7. PERFORMING ORGANIZATION NAME(S) AND ADDRESS(ES)
Environmental Research Institute of Michigan (ERIM)
P.O. Box 134001
Ann Arbor, MI 48113-4001

8. PERFORMING ORGANIZATION REPORT NUMBER
255700-4-F

9. SPONSORING/MONITORING AGENCY NAME(S) AND ADDRESS(ES)
AMSRL-SS-CC
2800 Powder Mill Rd.
Aldaphi, MD 20783-1197

10. SPONSORING/MONITORING AGENCY REPORT NUMBER
DAAL01-93-C-0074

11. SUPPLEMENTARY NOTES

12a. DISTRIBUTION/AVAILABILITY STATEMENT
N/A

12b. DISTRIBUTION CODE

13. ABSTRACT (*Maximum 200 words*)

This document is the final report for the study on the Multi-Aperture Synthesis Radar (MASR) concept. This report includes a description of the MASR system architecture, two point designs, and a performance comparison between the MASR concept and the existing SAR-P system. The report also discusses the MASR algorithm verification and presents MASR algorithm simulation results.

14. SUBJECT TERMS

15. NUMBER OF PAGES
62

16. PRICE CODE

17. SECURITY CLASSIFICATION OF REPORT	18. SECURITY CLASSIFICATION OF THIS PAGE	19. SECURITY CLASSIFICATION OF ABSTRACT	20. LIMITATION OF ABSTRACT
Unclassified	Unclassified	Unclassified	

CONTENTS

FIGURES

TABLES

MULTI-APERTURE SYNTHESIS RADAR COMPARATIVE STUDY

1.0 INTRODUCTION

This document is the final report for the study on the Multi-Aperture Synthesis Radar (MASR) concept. This report includes a description of the MASR system architecture, two point designs, and a performance comparison between the MASR concept and the existing SAR-P system. The report also discusses the MASR algorithm verification and presents MASR algorithm simulation results.

1.1 BACKGROUND

Autonomous wide area search, identification, and accurate geolocation of targets is an emerging sensor application. On a weapons delivery platform, a sensor can guide a weapon with surgical accuracy, giving the advantage of a precision strike capability. On a reconnaissance platform, an autonomous sensor can quickly provide wide area surveillance far beyond visual range. This capability can be achieved by long-range standoff of manned vehicles or by unmanned penetrating platforms. The latter saves lives but requires miniaturized, economical sensors consistent with smaller, possibly expendable, platforms.

Fine resolution imagery (defined as many resolution cells per target) is necessary for accurate target identification. Processor size is proportional to the number of processing operations on each cell multiplied by the cell rate; the cell rate is the product of velocity and swath width in units of resolution. Typical systems require fine resolution processing of all pixels in a swath. The MASR approach investigates an alternative to brute force imaging of a wide swath at fine resolution.

Today's fine resolution SAR sensors are large and expensive, making them affordable only to large fighting units like an army corps. Smaller, less expensive sensors are needed for division and brigade commanders with which to set their own priorities and pick their own targets. The key is to design economical sensors with high pixel throughput per unit size, weight, and power using available component technology.

1.2 SUMMARY

Multi-Aperture Synthesis Radar (MASR) is a novel sensor architecture designed to meet size and power constraints of Army missions requiring real-time, automatic target recognition (ATR) from SAR images. It partitions the data in space, time, and frequency to relieve peak data rates and conserve processing resources. Partitioned data is processed in stages to produce progressively finer resolution. Partitioning also permits the use of a parallel pipe-line architecture for the sensor and ATR. The whole seeker can be built from modules that can be reconfigured in real-time to operate in alternate modes. Single channel, fine resolution imagery can be replaced by multiple coarse resolution image channels to operate in monopulse, 3-D, or Dual Phase Center Aperture (DPCA) moving target detection modes. All real time systems are designed to meet some worst case scenario. For a typical SAR system, the real-time image formation processing operations can easily number in the billions of operations per second. The MASR approach reduces the peak processing requirement, making an affordable, realizable packing solution more achievable.

The basic MASR philosophy is to process the entire scene at coarse resolution using the polar format algorithm and only process small, fine-resolution image chips which coincide with coarse resolution target detections. The benefits of this processing approach are greatest with a sparse tar-

get density, which is typically encountered, or when detecting a few high value targets among low value targets with a higher density. The fewer targets detected per square kilometer, the less processing power required to generate target chips. The reserve processing power can then be used to increase the area coverage rate. MASR will, however, lose its advantage if more than 30 targets are detected per square kilometer. A side benefit of MASR is the potential target screening accomplished by the processor. The MASR concept will also reduce the radar hardware requirements by dividing the range bandwidth into 10 parts, each part with 1/10th the total bandwidth, and increasing the PRF by 10. This will maintain average power on the scene, but reduce peak power and data rate requirements.

Two parametric designs were developed for MASR with performance, such as fine resolution and operating frequency, similar to SAR-P. Both point designs illuminated a 2 km swath but the first design processed only 0.5 km, which is the same as SAR-P, while the second design processed the entire 2 km.

The MASR point design 1 and SAR-P systems were compared on the basis of weight, volume, power, processor operations, pixel rate and image quality. There are some hardware advantages for the MASR design. The transmitter will be smaller because of lower peak power requirements. The waveform generator, A/D converter and data buffer will be smaller and consume less power because of lower peak data rate requirements. The processor will require less weight, volume and power since fewer operations are required per scene. The system wide hardware savings in weight, volume and power of MASR over SAR-P are 16.2%, 15.4%, and 12.1% respectively.

There are fewer processor operations for the MASR design for the same area coverage as SAR-P. The total operations for fine resolution SAR-P processing are 3.6 Gflops. The total operations for equivalent MASR processing using the polar format algorithm are 2.3 Gflops which is 37% fewer than the SAR-P algorithm. There is an additional advantage of 3% to 6% using the MASR dual resolution approach if fewer than 30 targets are detected. The dual resolution approach becomes a disadvantage if more than 30 targets are detected. Pixel rates, which were compared on the basis of equivalent search areas, were estimated to be 6.2 M pixels/sec using 1.5 pixels/IPR. The pixel rate improvements over SAR-P are 16.2%, 15.4%, and 12.1% for pixels/sec per unit weight, volume and watt, respectively.

The MASR algorithm was verified in one dimension using simulated targets and in two dimensions using real radar data. The MASR main lobe responses are equivalent to SAR-P with a -3dB width of 1P and a -18dB width of 2P; however, the MASR far out sidelobes, which are elevated 15dB from typical 35dB Taylor weighted results, could be detected as false alarms. The MASR background noise was also elevated by 3dB more than SAR-P.

1.3 CONCLUSIONS

The MASR approach to the SAR-P system concept has benefits for the application of unmanned airborne vehicles (UAV). The MASR hardware architecture has some inherent savings in weight, volume, and power consumption. A portion of the MASR processing approach provides significant savings in processor requirements; this approach uses the polar format algorithm to eliminate scatterer motion through resolution cells and dual-resolution processing to reduce the number of fine resolution pixels generated. The polar format algorithm offers significant improvement in processing throughput. The implementation chosen for the dual-resolution processing, however, provided only a small advantage over conventional polar format processing when fewer than 30 targets per scene are detected. This small savings resulted in some degradation of image quality; consequently the dual-resolution MASR processing approach is not recommended.

2.0 PROGRAM OBJECTIVE

ERIM has developed a novel sensor architecture called Multi-Aperture Synthesis Radar (MASR). The goal of the sponsored program was to perform a series of studies to compare the MASR architecture with the SAR-P system using modern components and evaluate the pros and cons associated with each. The results of the studies will help the Army select optimal signal/data processing technologies and concepts to locate and engage the enemy in real time under all battle-field conditions.

The MASR program included three major tasks. During the first task, the Contractor became familiar with the proposed SAR-P radar and prepared two MASR point designs which provide the same geometrical coverage rate, image resolution, and operating frequency as the SAR-P. During the second task, the Contractor made an objective study of the pros and cons of MASR Point Design 1 and the SAR-P. The third task was the verification of the MASR processing approach.

3.0 POINT DESIGNS

3.1 MULTI-APERTURE SYNTHESIS RADAR DESCRIPTION

Traditional synthetic aperture radars (SAR) obtain fine azimuth resolution by moving the sensor and recording coherent data samples along the flight path. The coherent summation of these samples provides fine azimuth resolution; this coherent summation is equivalent to the synthesis of a large antenna aperture. MASR applies similar techniques to the frequency and space domains as well. The MASR approach distributes data acquisition and processing over time so that the peak data rates approach their average values, thus achieving a higher pixel throughput per unit power and weight. The slower clock rates for the digital portions of the system result in lower power consumption and reduced processor weight since most of weight is used for heat removal.

Careful selection of MASR parameters provides an optimal match between components and requirements. The input data is segmented and multiplexed in time and frequency to provide a modular, parallel pipeline architecture in the processor. Data segmentation is optimized to fully utilize component capabilities and reduce data rates so that it is possible to build wide area search, fine-resolution SAR/ATR seekers using component specifications found in present workstation computers. The MASR concept involves new signal management methods which start with data collection and continue through adaptive processing.

Figure 3.1 is a sketch of the geometry for the MASR application studied in this program. An unmanned aerial vehicle (UAV) is collecting data over a continuous strip to locate critical mobile targets. A wide swath, all-weather, day/night capability is required from a radar restricted in weight and prime power. Detection and identification of stationary targets is required, and a target positioning capability is desirable. The MASR approach to the problem is to form a strip map with course resolution which minimizes the processing requirements. A target cueing algorithm is applied to search the strip map for areas likely to contain targets of interest. Small, fine resolution "chips" corresponding to target detections are then processed for target identification; see Figure 3.2. It is anticipated that the search resolution will be four times the identification resolution.

The conventional approach to obtaining fine range resolution with a chirp waveform is to transmit the entire bandwidth required for the resolution during a single pulse as sketched in Figure 3.3a. With the conventional approach, the minimum operating range limits the maximum allowable pulse width. Long pulse widths are desirable to increase the average transmitted power. With the MASR approach, depicted in Figure 3.3b, a stepped frequency chirp is used. With this approach, the transmitted bandwidth is divided by a factor N, and one Nth of the bandwidth is transmitted on N successive pulses. This approach provides the same resolution as the conventional approach with an effective pulse width which is N times as long. The longer effective pulse length reduces the peak power required by the transmitter by a factor of N and also reduces the FM rate of the chirp signal so that the bandwidth of the deramped returns is reduced by a factor of N. The lower A/D rates permit improved A/D converter performance.

The generation of the signal bandwidth with multiple narrow band chirp steps makes it possible to avoid the frequency multiplication circuitry found in conventional designs with wide band chirp waveforms and the associated phase noise degradation associated with frequency multiplication, which results in a phase noise increase in dB of 6 times the number of multiplication steps. The quantization noise obtained with the initial chirp generation is also lower because of the slower clock rates.

With the conventional processing approach, the entire polar formatted phase history is processed at one time to form a fine resolution image, as shown in Figure 3.4. With the MASR
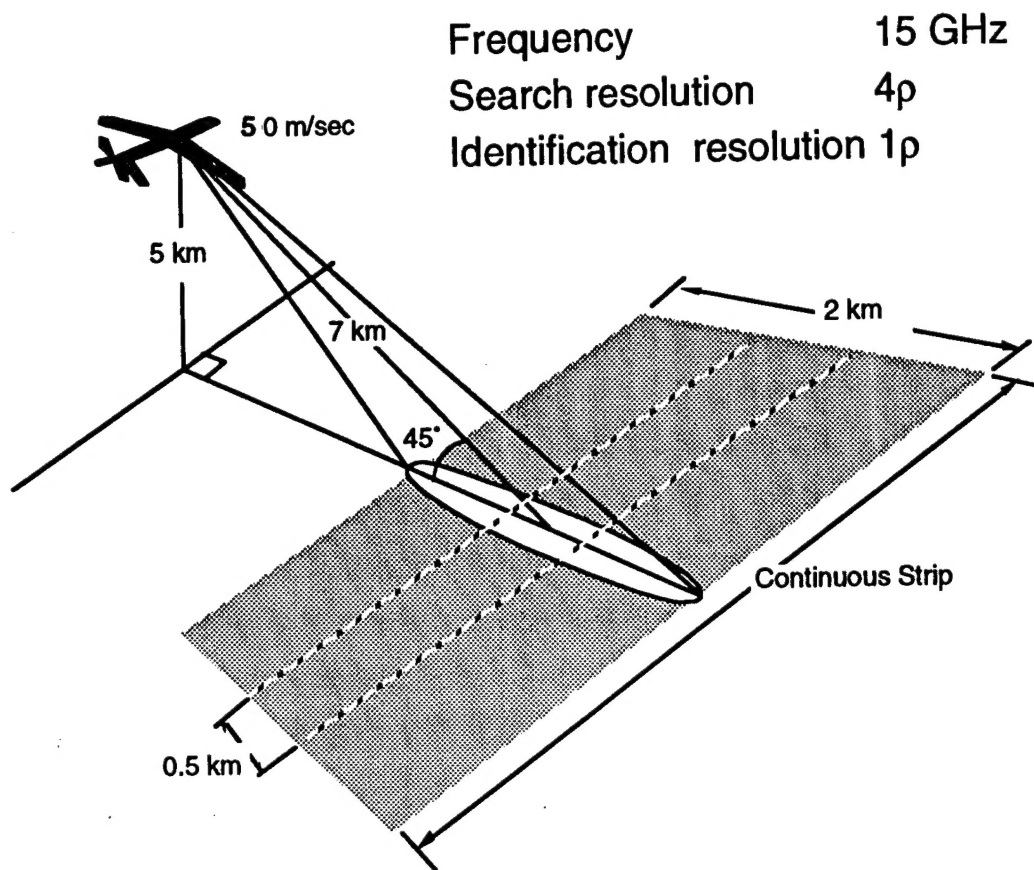
4
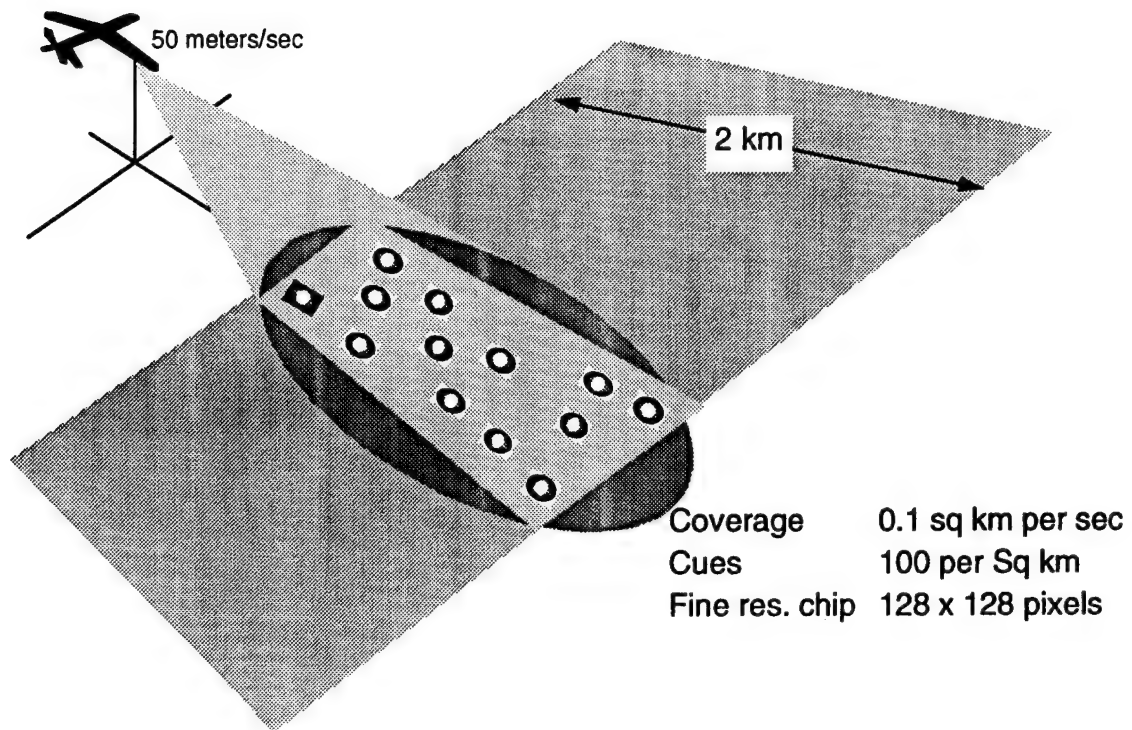
Figure 3.1 Typical MASR Geometry
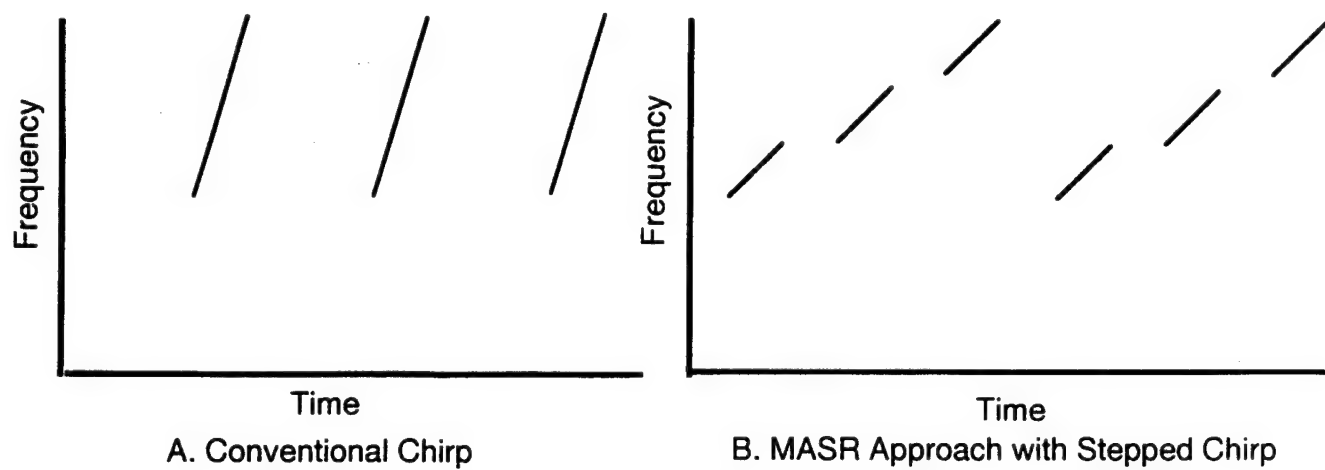
Figure 3.2 Fine Resolution Chips

Figure 3.3 Transmitted Waveforms for Fine Range Resolution

approach shown in Figure 3.5, the polar-formatted phase history is divided into N by N sections, and each is processed with a two-dimensional FFT to provide an image whose resolution is N times the resolution which would be obtained by processing the entire phase history. The computations required to process the N by N polar formatted phase histories is less than computations required to process the entire phase history at one time to provide a a single fine-resolution image of the entire scene.

A target cueing algorithm searches the coarse resolution images for areas likely to contain targets of interest, and a limited number of areas are selected for further processing. As shown in Figure 3.5 for N equal to 2, small chips of these areas are selected from the coarse resolution images; the coarse -resolution image chips of a given area are accurately registered because they originate from different sections of the same fine resolution phase history. Data from the coarse resolution chips is then coherently combined to form chips whose resolution is equivalent to that obtained from the entire polar formatted phase history. Conventional target recognition algorithms will then be applied to the fine resolution chips. Although the polar formatted phase history in Figures 3.4 and 3.5 is divided into four parts for simplicity, the polar formatted phase history is divided into 16 parts for the baseline MASR Point Design 1 where the resolution of the coarse images is four times the fine resolution which can be obtained from the entire phase history.

3.2 POINT DESIGN REQUIREMENTS

Section C.2 of the Statement of Work lists the requirements for the MASR Point Designs. The contractor must provide two point designs of SAR systems based on the MASR architecture: the elevation beamwidth of the antenna for both designs shall cover at least 2 km on the ground plane. MASR Design 1 shall provide the same geometrical coverage and have the same fine resolution and frequency as the proposed SAR-P. MASR Design 2 shall be similar to the first, but the range swath imaged shall be expanded to 2 km on the ground plane.

As a minimum, the point designs shall designate values for the parameters listed below in Table 3.1. The MASR concept uses a dual resolution approach, and the contractor design shall use a fine resolution mode with resolution P equal to that of the SAR-P, and a coarse resolution mode with resolution equal to 4P. To scope the hardware requirements, the contractor shall assume that the maximum density of the high resolution target detections is 100 per square kilometer. (This requirement is really driven by the false alarm rate assumed for the target cueing algorithm.) The contractor shall also assume that a fine resolution chip is 128 by 128 pixels and that the pixel oversampling of the impulse response is 1.5. The contractor shall estimate the size and weight of the components needed and explain the assumptions made in generating these estimates.

Table 3.1. Point Design Parameters

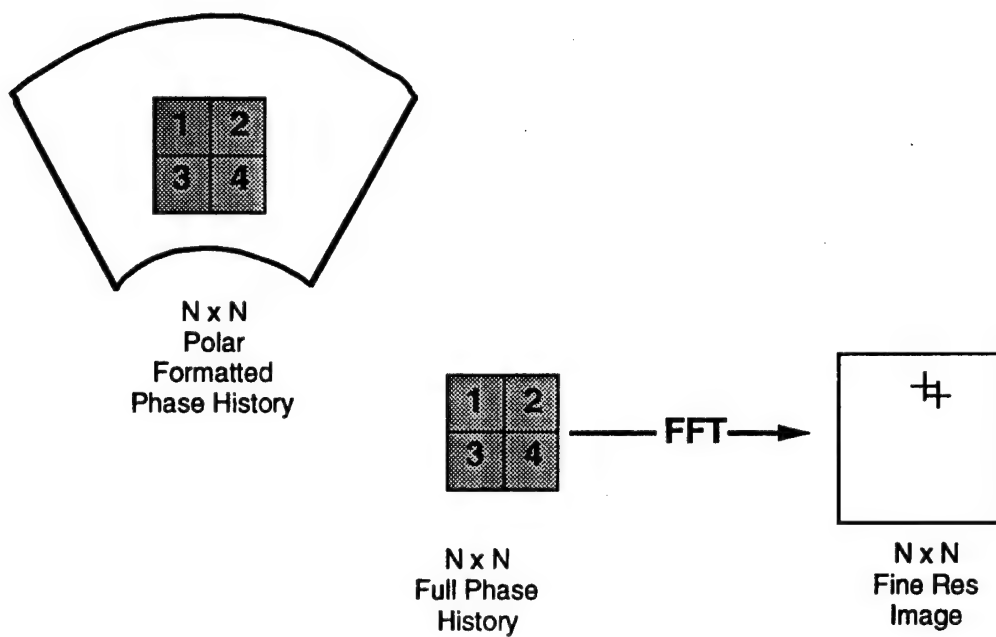|	
Receiver Noise Figure	I & Q or Range Offset Video
Pulse Width	Presumming Ratio
Transmitted Bandwidth	No. Fast Time Samples
Antenna Beam Widths	No. Slow Time Samples
Antenna Gain	System Losses
Transmitted Power	PRF
A/D Sample Rates	Scene Size in Pixels
Memory Sizes	

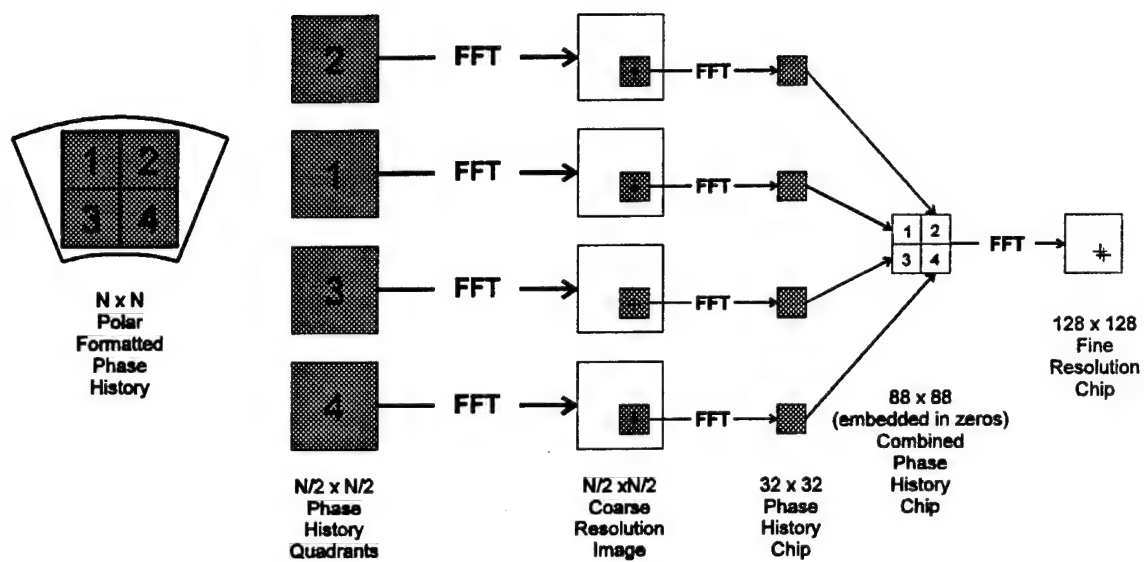Figure 3.4 Fine Resolution by Conventional Processing Approach

Figure 3.5 Fine Resolution by MASR Approach

3.3 POINT DESIGNS

3.3.1 Parameters

3.3.1.1 Geometry

For the point designs, it will be assumed that an unmanned aerial vehicle (UAV) will carry the radar, and that the ground speed of the UAV is 50 m/s. Figures 3.6 and 3.7 are sketches of the geometries for the two point designs. The UAV is at a height of 5 km, and the center of the swath illuminated is at a depression angle of 45 degrees. The illuminated swath of the transmitted beam is 2 km for both designs; however, the swath width actually mapped is 0.5 and 2.0 km for Point Designs 1 and 2, respectively. The ellipses in the figures mark the contours of the receiving antenna patterns. Maximum antenna dimensions of 0.26 m in azimuth by 0.25 m in elevation were assumed to conform with typical aperture constraints for a UAV. For the 0.5 km swath, the receive beam makes use of the full allowable aperture, and a single beam is sufficient to cover the desired 0.5 km swath. Two receiving beams offset in elevation are necessary to cover the 2.0 km swath required in MASR Point Design 2.

3.3.1.2 Resolution

The MASR will transmit a stepped chirp waveform, and the slant-range resolution ρ_r depends on the transmitted bandwidth ΔB spanned by the ten chirp pulses.

$$\rho_r = \frac{k_r c}{2 \Delta B} \tag{1}$$

Here k_r is the excess bandwidth factor, and c is the velocity of light. The excess bandwidth factor depends on the aperture weighting used for sidelobe reduction: a value of 1.20 is typical. The bandwidth ΔB will be about 600 MHz for the fine resolution 1P. The range resolution in the ground plane equals the slant-plane resolution multiplied by the cosecant of the grazing angle.

The azimuth resolution ρ_a depends on the wavelength λ and the integration angle $\Delta\theta$

$$\rho_a = \frac{k_a \lambda}{2 \Delta \Theta} \tag{2}$$

Here k_a is the excess angle factor, which depends on the aperture weighting to reduce azimuth sidelobes and any broadening resulting from azimuth phase and amplitude errors. A value of 1.2 to 1.3 is typical. At a center frequency of 15 GHz, the integration angle $\Delta\Theta$ will be about 40 mrad. At a slant range of 7 km, the aperture time will be about 5.6 seconds for 1P resolution and 1.6 seconds for 4P resolution.

For uniform azimuth resolution across each image patch, the azimuth patch size must be chosen such that each scatterer in the patch remains illuminated over the cone angle interval required to support the desired azimuth resolution of equation (2). Given the azimuth antenna beamwidth β_a, $\Delta\Theta$ from equation (2), and the slant range (R_a), the maximum azimuth patch size is given by

$$\Delta x = 2R_a \left[\tan\left(\frac{\beta_a}{2}\right) - \tan\left(\frac{\Delta\Theta}{2}\right) \right] \tag{3}$$

In the MASR system, Δx is 380 meters for Point Designs 1 and 2.

Figure 3.6 Geometry for MASR Point Design 1
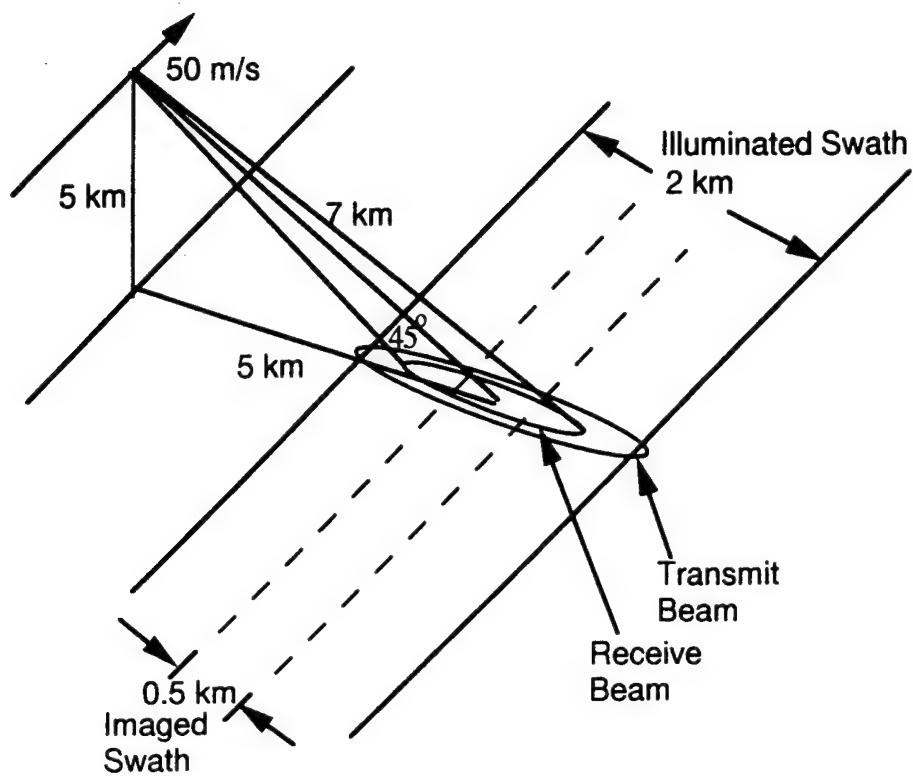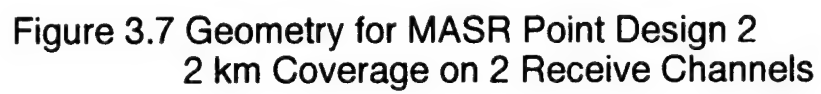0.5 km Coverage on 1 Receive Channel

12

Figure 3.7 Geometry for MASR Point Design 2
2 km Coverage on 2 Receive Channels

The length L_p of the synthetic aperture required to collect an azimuth patch size of 380 meters is

$$L_p = 2R_a \tan\left(\frac{\Delta\Theta}{2}\right) + \Delta x \qquad (4)$$

For the MASR fine resolution mode, L_p is 660 meters; for coarse resolution, L_p is 450 meters. For a platform velocity of 50m/s, the patch integration times are 13.2 and 9.1 seconds, respectively.

3.3.1.3 Transmitted Waveform

The 600 MHz of transmitted bandwidth will be obtained from 10 stepped chirp pulses, each of which covers a 60 MHz band.The transmitter PRF will be 10,000 Hz, but the effective PRF for each 60 MHz step will be only 1000 Hz. The transmitted pulse widths will be 30.98 and 27.69 μsec for the 0.5 and 2.0 km swaths, respectively. The corresponding transmitter duty cycles are 30.98% and 27.69), respectively.

The minimum operating range with the 27.69 μsec pulse width will be 4.3 km with a 1 μsec recovery time after transmission. For each 60 MHz transmit band, the pulse repetition interval is 1000 μsec, and the maximum allowable delay for the received pulse is 1000 μsec minus the pulse width; this delay corresponds to an unambiguous range interval of about 146 km. With the 5.38 degree azimuth antenna beamwidth, which will be discussed later, the Doppler bandwidth of the signal spectrum will be 466 Hz at broadside at the 50 m/s UAV ground speed. The 1000 Hz PRF for each chirp pulse is high enough so that azimuth ambiguities are not a problem until the sensor ground speed exceeds 80 m/s.

3.3.1.4 Antenna Beamwidth and Gain

The limitations on the antenna beamwidth are the maximum size of the aperture available on the UAV, the azimuth resolution required, and the swath width. As mentioned previously, the maximum physical aperture available is 26 cm in azimuth by 25 cm in elevation. For an aperture of length D and weighting for sidelobe reduction to -35 dB, the approximate beamwidth $\Delta\beta$ is

$$\Delta\beta \cong \frac{1.2\lambda}{D} \qquad (5)$$

where λ is the wavelength, assumed to be 2 cm for the MASR. For the 26 cm azimuth aperture, the azimuth beamwidth will be about 5.38 degrees. For the strip-map SAR mode, the azimuth aperture must not exceed twice the azimuth resolution; for the MASR with 30 cm resolution, the azimuth aperture is limited to 60 cm, or about twice the physical aperture available.

The required swath width limits the allowable elevation beamwidth of the antennas. For the geometries of Figures 3.6 and 3.7, the requirement that the transmitting antenna illuminate a 2 km swath results in an 11.5 degree transmit beamwidth for both point designs. A single receive beam is sufficient to cover the 0.5 km swath; the elevation beamwidth will be 5.6 degrees, the minimum beamwidth available with the 25 cm vertical aperture. Two receive beams offset in elevation are required to cover the 2 km swath; the widths of these beams in elevation will also be 5.6 degrees.

The gain G of an antenna aperture depends on the azimuth and elevation beamwidths, Θ_{az} and Θ_{el}; the approximate gain is

$$G \cong \frac{28000}{\Theta_{az}\Theta_{el}} \qquad (6)$$

Equation 6 assumes an antenna efficiency of about 60%. The transmitting antenna, which has elevation and azimuth beamwidths of 11.5 and 5.38 degrees, will have a gain of approximately 26.0 dB. For reception, the beamwidths in elevation and azimuth are 5.6 and 5.4 degrees, resulting in a gain of about 29 dB.

3.3.1.5 Transmitter Power

A solid state transmitter with a peak power of only 10 W (40 dBm) will be used for both point designs. From the duty cycles in Section 3.3.1.3, the average transmitted powers for Point Designs 1 and 2 will be 3.10 and 2.77 W, respectively. The effective average powers for signal-to-noise ratio calculations will be 2.86 and 2.27 W, respectively, because the recorded pulse width is slightly less than the transmitted pulse width.

3.3.1.6 The Video Bandwidth and the Data Recording Rate

The slant-range swath width ΔR and the chirp rate determine the video bandwidth, B_v, which is given by

$$B_v = \frac{2\gamma\Delta R}{c} \qquad (7)$$

Here c is the velocity of light, and γ is the FM rate of the chirp signal, where

$$\gamma = \frac{\Delta f}{\tau_{rec}} \qquad (8)$$

Here Δf is the frequency change during a pulse, 60 MHz, and τ_{rec} is the width of the recorded pulse. The width of the recorded pulse equals the width of the transmitted pulse minus the swath time, $2\Delta R/c$. Taking the 45 degree grazing angle into account, the swath times are approximately 2.35 and 5 μsec for 0.5 and 1.0 km ground swaths, and the recorded pulse widths are 28.6 and 22.7 μsec.

From equation 8, the FM rates are 2.095 and 2.64 $\times 10^{12}$ Hz/s for the 0.5 and 1.0 km swaths. From equation 7, the video bandwidths are 4.92 and 13.17 MHz, respectively. To satisfy the Nyquist criterion with real data sampling, the sampling rate of the A/D converter, f_s, must exceed twice the highest frequency present. A/D converter sampling rates of 12.0 and 30.0 MHz will be used for the 0.5 and 1.0 km swaths, respectively.

The number of data samples per pulse N_p equals the product of the A/D converter sampling rate and the recorded pulse width

$$N_p = f_s \tau_{rec} \qquad (9)$$

The samples per pulse are 343 and 681 for the 0.5 and 1.0 km ground swaths. The throughput, f_{TP}, equals N_p times the PRF

$$F_{TP} = N_p PRF \qquad (10)$$

15

With the 10 kHz PRF, the throughputs are 3.43 and 6.81 Megasamples/sec for the 0.5 and 1.0 km swaths, data rates that can be readily dealt with.

3.3.1.7 Hardware Parameter Summary

Table 3.2 summarizes the hardware parameters for the MASR point designs. The previous subsections have discussed the parameters in Table 3.2 except for the systems losses. The 7.6 dB system losses include 1.4 dB for the two-way propagation losses, 1 dB for the transmitter hardware losses, 3 dB for the receiver hardware losses, and 1.2 dB for processing loss.

Table 3.2 MASR Hardware Parameters

Parameter	Point Design 1	Point Design 2	Units
SAR Mode	strip map	strip map	
Resolution	1P fine, 4P coarse	1P fine, 4P coarse	
Center Frequency	15	15	GHz
Swath Width	0.5	2.0	km
Scene Size	0.5 by 0.38 2500 by 1900	2.0 by 0.38 10000 by 1900	km pixels
Receive Channels	1	2	
Antenna BW Trans	11.5 el, 5.38 az	11.5 el, 5.38 az	degrees
Gain Trans Ant	26	26	dB
Receive Beams	1	2	
Antenna BW Rec	5.6 el, 5.38 az	5.6 el, 5.38 az	degrees
Gain Rec Ant	29	29	dB
Transmitter Power	10 peak, 3.1 av	10 peak, 2.8 av	W
Trans PRF	10	10	kHz
PRF/Chirp Step	1	1	kHz
Trans Pulse Width	31.0	27.7	μsec
Recorded Pulse	28.6	22.7	μsec
FM Rate	2.095×10^{12}	2.64×10^{12}	Hz/s
Total Bandwidth	600	600	MHz
Noise Figure	3.5	3.5	dB
Losses	7.6	7.6	dB

Table 3.2 MASR Hardware Parameters (Continued)

Parameter	Point Design 1	Point Design 2	Units
A/D Resolution	8	8	bits
A/D Sample Rate	12	30	MHz
Sampling Method	Range Offset	Range Offset	
Samples/Pulse	343	681	
Throughput	3.43	6.81	Megasamples/s
Slow Time Samples (Pulses)	9100 (coarse) 13200 (fine)	9100 (coarse) 13200 (fine)	
Presum Ratio	5 (coarse and fine)	5 (coarse and fine)	
Memory Size	50	200	Megabytes

3.3.1.8 The Additive Noise Level

With a SAR, the radar receiver and processor act like a matched filter for the transmitted waveform, and the radar equation provides the signal-to-noise ratio after processing

$$\frac{S}{N} = \frac{P_{av}G_tG_r\lambda^2\sigma T_i}{(4\pi)^3 R^4 kT_o FL} \tag{11}$$

Here P_{av} is the average power, G_t and G_r are the gains of the transmitting and receiving antennas, λ is the wavelength, σ is the radar cross section of the target, T_i is the integration time, R is the slant range, k is Boltzmann's constant (1.38×10^{-23} J/K), T_o is 290 K, and FL is the product of the noise figure times the losses. Setting S/N =1 in equation 11, solving for σ, and dividing σ by A, the area of a resolution cell provides σ_n, the equivalent reflectivity of the additive noise. The resolution cell area A is given by

$$A = \rho_r\rho_a\csc\psi \tag{12}$$

In equation 12, ρ_r and ρ_a are range and azimuth resolutions, and ψ is the grazing angle. Thus,

$$\sigma_n = \frac{(4\pi)^3 R^4 kT_o FL}{P_{av}G_tG_r\lambda^2 T_i\rho_r\rho_a\csc\psi} \tag{13}$$

At a 7 km slant range, σ_n for Point Design 1 was -30 dB for P resolution and -36.5 dB for 4P resolution. For Point Design 2, the corresponding values of σ_n were -29 dB for P resolution and -35.5 dB for 4P resolution. Since σ_o, the reflectivity of the terrain, is usually between -20 and -10 dB, σ_n for both point designs is low enough to provide good ground painting in the images.

17

3.3.2 System Configuration

3.3.2.1 Data Collection

The MASR design employs polar format processing. During polar formatting, the received data segments are placed on a common rectangular grid taking into account the radar position change between pulses. The swath is divided into contiguous azimuth patches, and the processing is performed in two cycles: a coarse resolution cycle with 4P by 4P resolution and a fine resolution cycle with P by P resolution. The coarse resolution cycle occupies a full-resolution aperture time, while the fine-resolution cycle occupies a time interval equal to the difference between the patch fly-by time and the full-resolution aperture time. Portions of the coarse resolution images selected by a target cueing algorithm are then recirculated through the fine-resolution processor to form target chips. Coarse resolution processing starts as soon as each quarter of the full-resolution aperture is processed.

During data collection, the antenna transmit and receive beams are pointed at midswath in elevation and at broadside in azimuth; in azimuth, the antenna pointing changes only to correct for yaw. The motion compensation point is fixed on the center of the patch, similar to the spotlight mode for a conventional SAR radar. At scene center, the antenna foot print is 664 meters wide, and the synthetic aperture length is about 300 m for 1 P resolution. A full phase history is collected for a patch some 364 m wide. During polar formatting in the processor, the data is low-pass filtered in azimuth to retain only data pertaining to the azimuth patch; data at higher Doppler frequencies is discarded, as is the phase history data which has not been collected for a full aperture. As mentioned previously, the PRF for each chirp step is high enough so that azimuth ambiguities are not a problem.

3.3.2.2 Block Diagram

Figure 3.8 is a simplified MASR system block diagram. Point Design 1 with the 0.5 km swath uses a single channel, while Point Design 2, which covers a 2 km swath with two 1 km segments, has two receiver channels. The second receiver channel, which is not shown in Figure 3.8a, will be identical to the first. The antenna aperture is split into two halves, and the transmitted beam uses only one of the aperture halves to provide the wide elevation beam needed to illuminate the 2 km swath. During reception, signals from the two half apertures are combined electronically by the beam forming network to provide one narrower beam for Point Design 1 or two narrower beams for Point Design 2. For Point Design 2, the two beams are offset in elevation so that each receive beam covers a 1 km swath and feeds one of the two receiver channels.

The waveform generator (WFG) provides the stepped chirp signal to the solid-state transmitter and the reference signal to the mixer after the low-noise receiver front end. The deramped returns from the mixer pass to the IF amplifier, and an A/D converter at the IF amplifier output digitizes the data at a sample rate of 12 or 30 MHz for the two point designs. After real-to-complex conversion, the data passes to an I and Q buffer, and motion compensation is applied at the buffer output. The processing blocks in Figure 3.8b and 3.8c will be discussed later.

3.3.2.3 Timing, Waveforms, and Signals

Figure 3.9 is a transmit-receive timing and frequency diagram. The two-way travel time to the near edge of the swath plus a 1 μsec recovery time limit the transmitted pulse width. The stepped chirp waveform is 10 pulses long, and each step has a 60 MHz bandwidth so that 600 MHz is transmitted during one cycle. Since the coarse resolution mode uses 150 MHz of bandwidth, the processor uses data from two and a half chirp steps for each coarse resolution image.
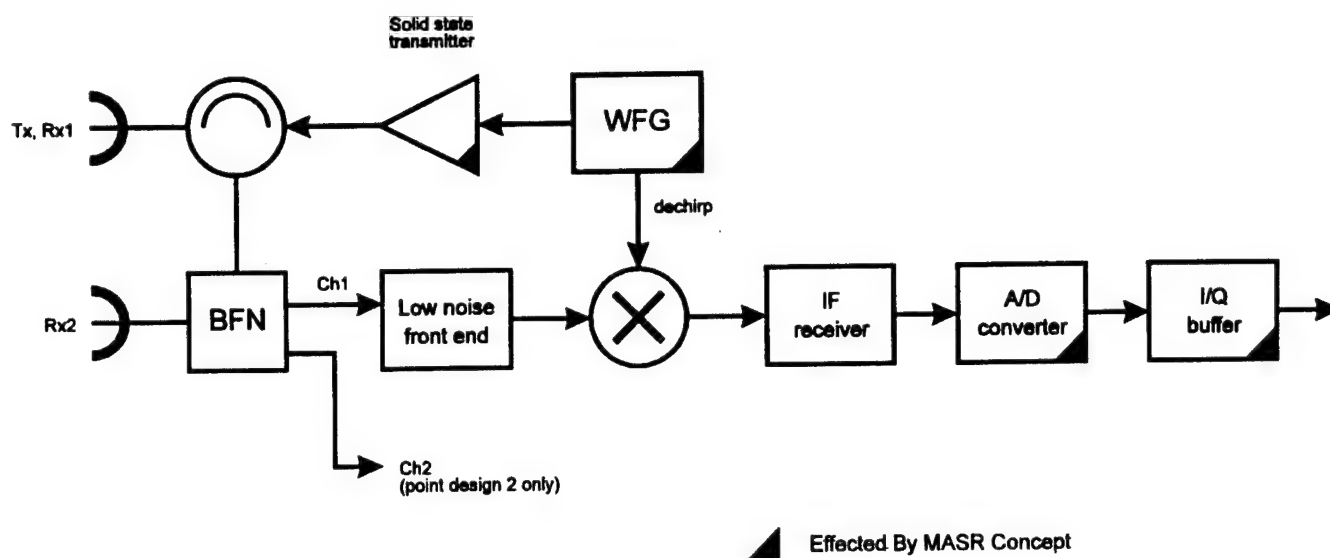
18

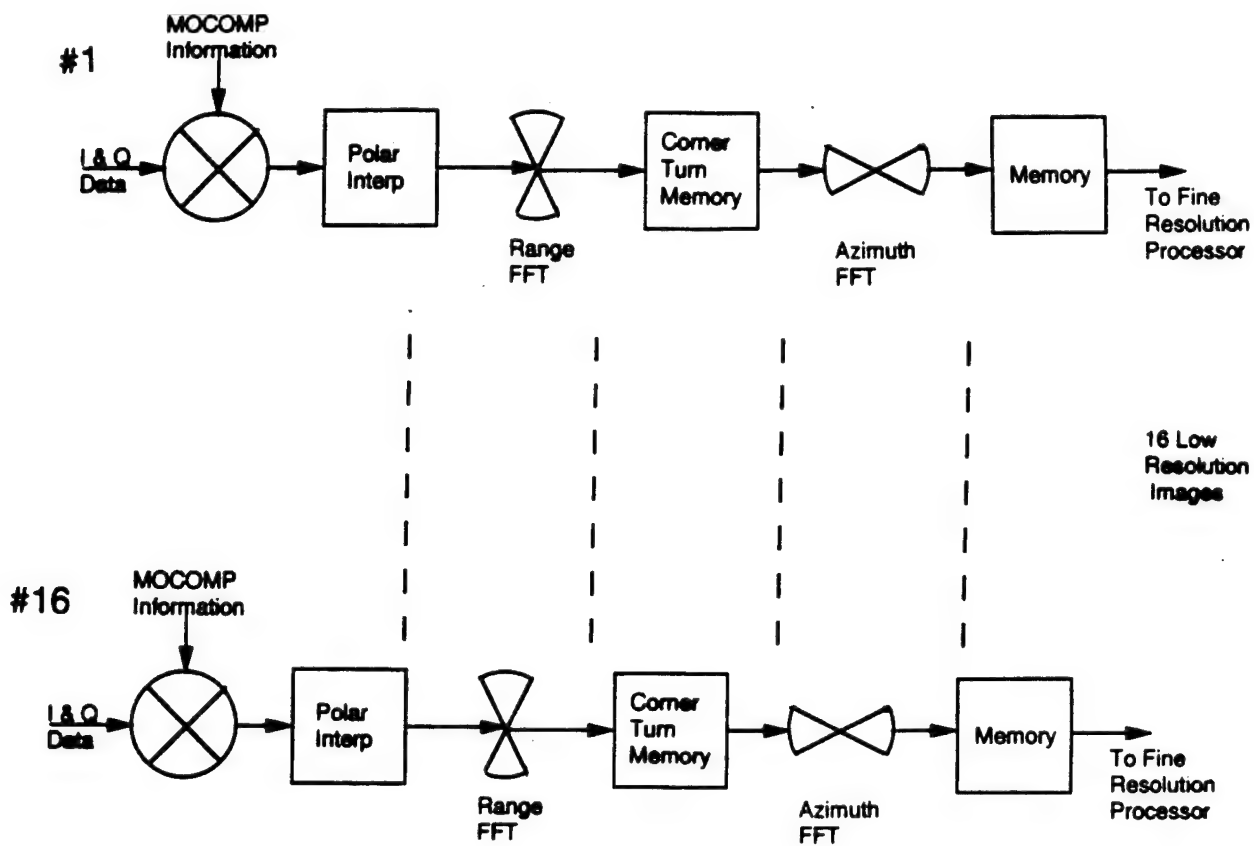Figure 3.8a MASR Hardware Block Diagram

Figure 3.8b. MASR Coarse Resolution Processor Block Diagram
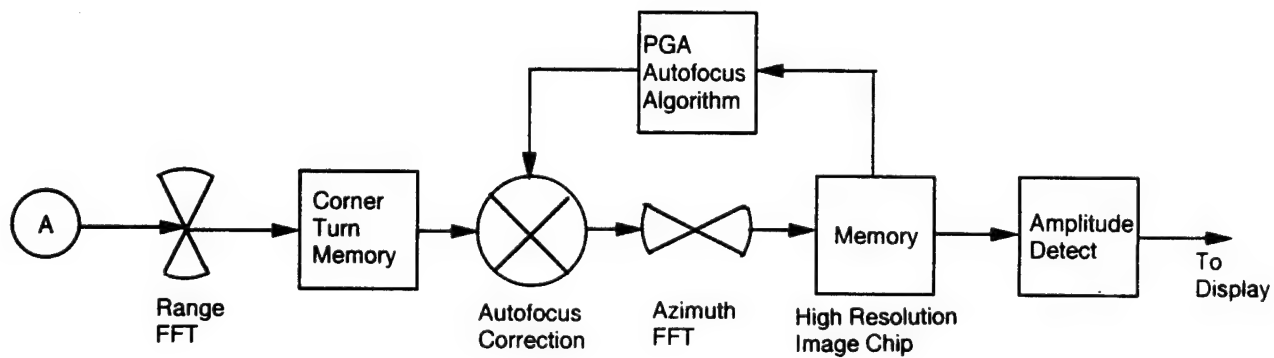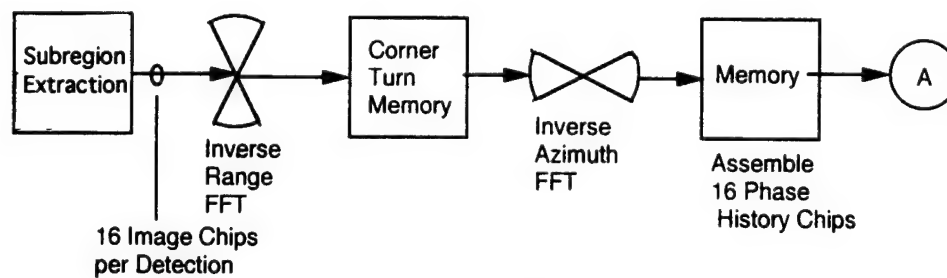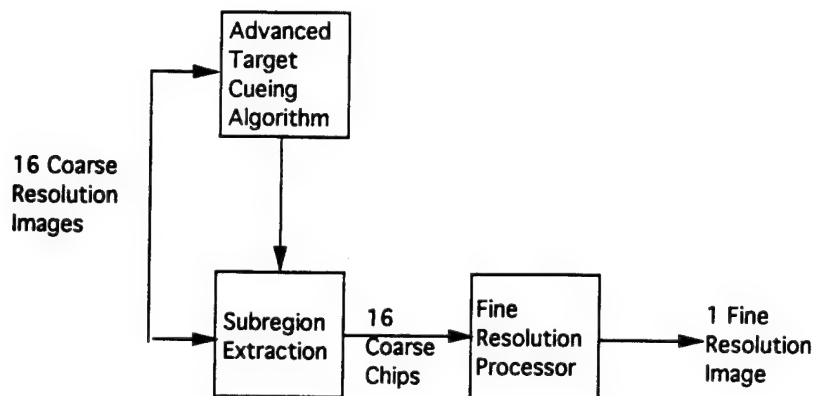16 Parallel Subaperture Processors

20

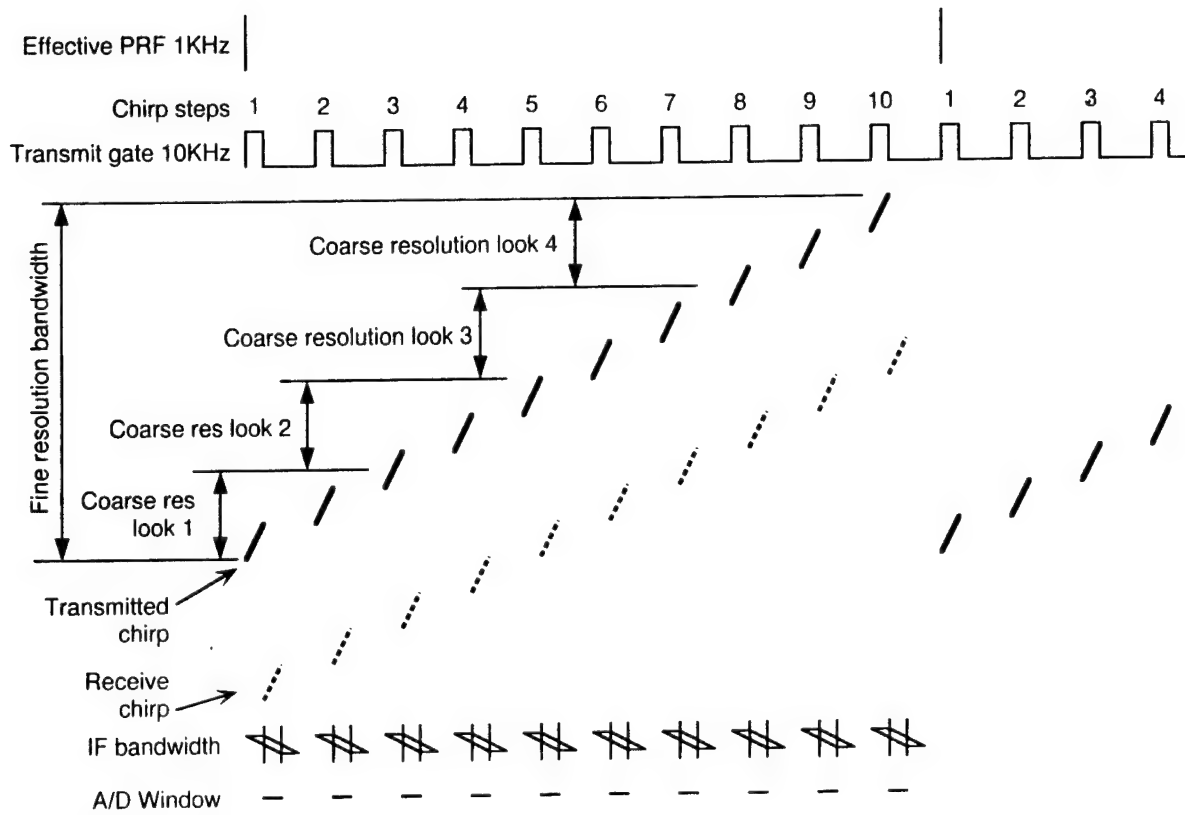Figure 3.8c MASR Fine Resolution Processor Block Diagram

Figure 3.9 MASR Transmit-Receive Timing Diagram

The linear FM signal transmitted during each pulse mixes with a delayed replica of the transmitted signal to deramp the returns; the time delay for the reference equals the two-way travel time to the scene center. The WFG synthesizes chirp signals digitally at an appropriate lower frequency, and the WFG output is then mixed with appropriate CW signals from the Timing and Frequency Generator (TFG) to upconvert the chirp signals to the appropriate frequency band. The center frequency of the reference signal for the receiver differs from the center frequency of the transmit signal by the desired center frequency of the IF amplifier.

The macro timing diagram in Figure 3.10 displays the time intervals for each of the processing steps discussed here and in the next section. Coverage is continuous as long as the azimuth patch width is longer than a full-resolution synthetic aperture and the patch processing time is less than the patch fly-by time, and both of these conditions are satisfied. The top line in Figure 3.10 represents the nth azimuth patch fly-by, and the second line is the aperture time for the four coarse-resolution azimuth looks. The fine-resolution aperture time is the sum of the aperture times for four coarse looks.

The IF center frequency equals one quarter of the A/D sampling frequency to facilitate the conversion of the real data centered at the IF carrier frequency to I and Q video data. This approach to obtaining I and Q data has the advantage that the I and Q channels after the digital conversion have a perfect amplitude and phase match. As shown in Figure 3.9, returns are digitized during the time interval when signals from the entire swath are present simultaneously. Although some energy over the time interval equal to the swath delay is wasted, processing is simplified with this recording technique.

In the preprocessor, the digitized video is converted to I and Q and buffered in a first-in-first-out (FIFO)memory. Data is read out of the FIFO memory at a nearly uniform rate which is much less than the A/D conversion rate because the recorded pulse width is much less than the 100 µsec pulse repetition interval. The conversion of the real data to I and Q and the first stage of motion compensation occur in real time. The FIFO memory introduces a latency of at least one transmitted pulse because a delay is necessary to wait for the motion data.

3.3.3 Processing

Strip map data is processed as a continuous sequence of spots. There are 16 coarse resolution processors which use polar format processing and form 16 coarse resolution images. These 16 coarse resolution images are the inputs to the fine resolution processors which form fine resolution image chips of cued areas containing potential targets.

3.3.3.1 The Coarse Resolution Cycle

The coarse resolution processor consists of 16 subaperture processors which process all the data from a patch in parallel; Figure 3.8b is a block diagram of the subaperture processors. Each subaperture processor receives the buffer output and the current motion data simultaneously, and motion compensation is applied at the processor input. At the first motion compensation stage, which is called range frequency adjustment, each input data vector is multiplied by a complex frequency vector to compensate for the radial shift in radar position and to place the scene center at zero range and Doppler frequency.

The polar formatting, which occurs in real time, is the next processing step: the input data form radial segments which are interpolated to form a uniform, rectangular output grid, as shown in Figure 3.11. The radial and angular locations of the input data samples are taken into account to match the actual radar position relative to the scene center at the time of the pulse to accomplish
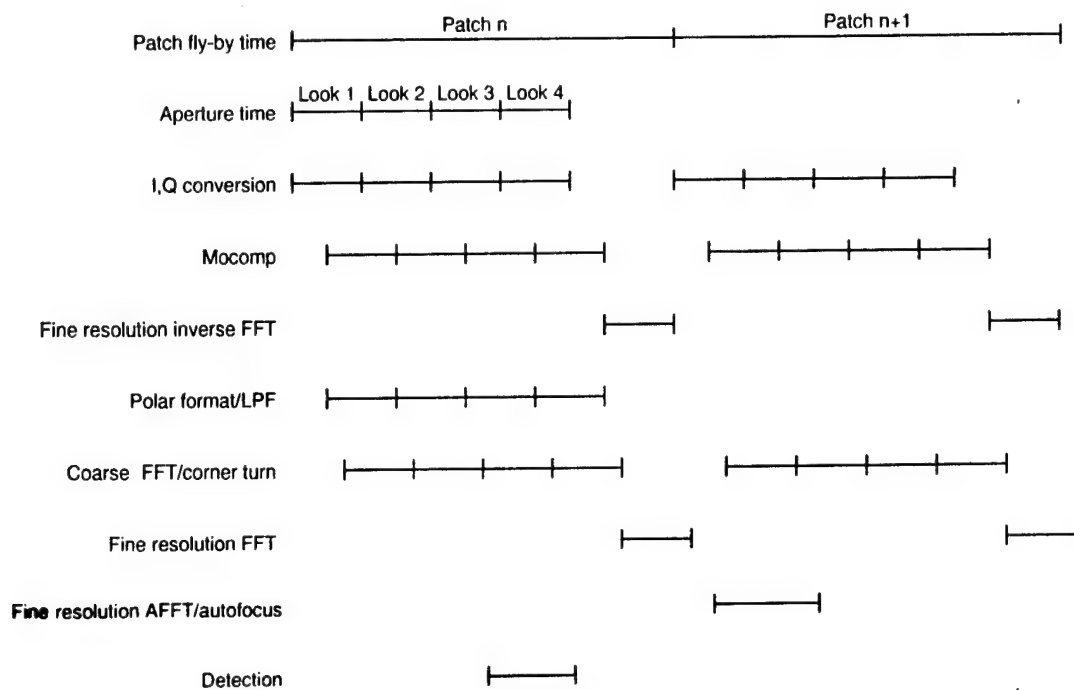
23

Figure 3.10 Macro Timing Diagram
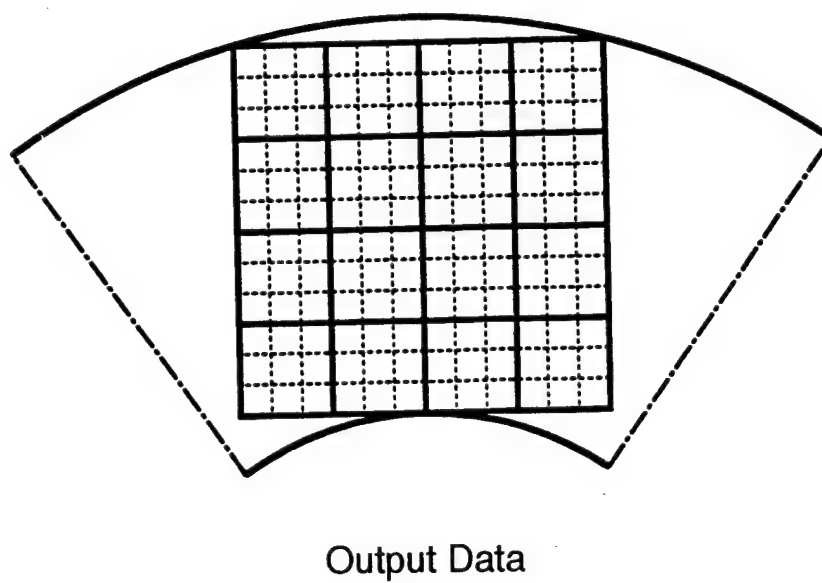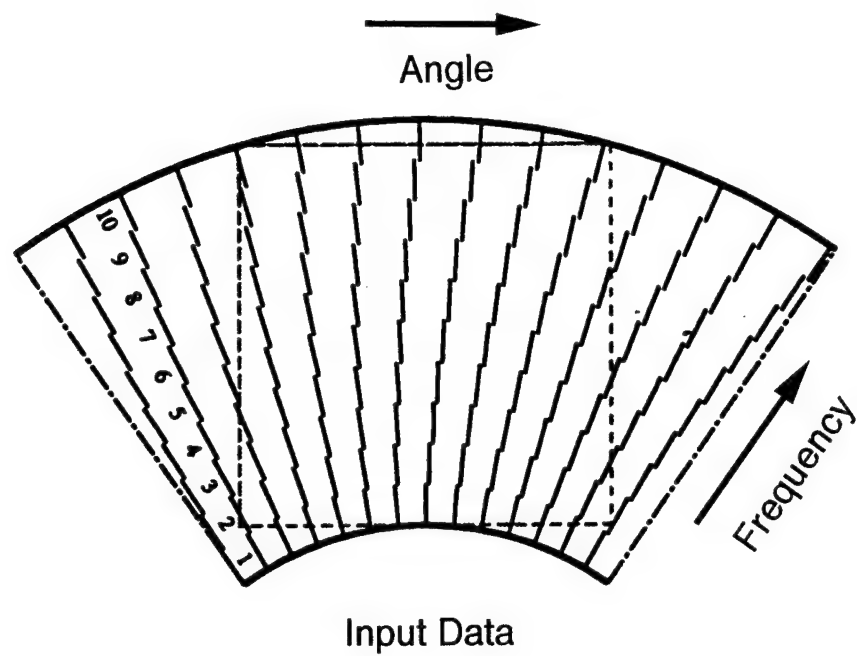
Angle

Input Data

Output Data

Figure 3.11 Polar Formatter Input and Output Data

25

the second stage of motion compensation, range and azimuth phase adjustment. The motion compensation system provides the required position information. Since the length of the azimuth filter in the polar formatter is eight cycles long, the latency introduced is 8 msec.

A two-dimensional FFT forms an image from the polar formatter output data. For the coarse resolution image, a range FFT (RFFT) is performed on one quarter of each polar formatted range record to provide four compressed range looks with 4P resolution. The coarse range FFT occurs in real time at the polar format output; it adds one PRF cycle (1.0 ms) of latency. Point Design 1 uses a 512 point range FFT, and Point Design 2 uses a 2048 point range FFT to generate the coarse range resolution data.

The range FFT output is buffered in the corner-turn memory where the rows and columns are interchanged to prepare the data for the coarse azimuth FFT (AFFT); this is performed when a sufficient number of azimuth records, one quarter of the fine resolution aperture, have accumulated in the corner-turn memory. Thus, the azimuth FFT adds one coarse resolution cycle of latency, one quarter of a fine resolution aperture time. The coarse azimuth FFT occurs at a rate which is faster than the real-time rate at the polar format output. The azimuth FFT length is 512 for both point designs. The coarse azimuth FFT requires one coarse resolution aperture time.

The processor output is 16 coarse resolution looks at the scene; each look results from a two-dimensional FFT taken over one sixteenth of the fine resolution aperture which has been divided by four in both range and azimuth. The total latency for each coarse resolution azimuth look is within two coarse resolution aperture times. The coarse resolution processing time for all sixteen looks equals one fine-resolution aperture time.

3.3.3.2 The Fine Resolution Cycle

The fine resolution processing cycle begins upon completion of the coarse resolution cycle. One of the 16 low resolution images is fed into a target cueing algorithm that selects small image areas, or chips, likely to contain targets of interest. Only these small image areas, or chips, are further processed to fine resolution. If the cueing algorithm identifies no target areas, then no fine resolution processing is performed. The exact nature of the target cueing algorithm must still be determined, but ERIM has developed algorithms for the detection and discrimination of targets in clutter on other programs

Reference[1] discusses detect on and discrimination algorithms developed at ERIM and describes test results on data collected from the Lincoln Laboratories Advanced Detection Technology Sensor (ADTS radar). The ADTS radar provides fully polarimetric, one-foot resolution data at Ka-band. These algorithms make use of three clutter features: spatial, contrast, and polarimetric. The MASR Point Design data is different in that the 4P resolution data sent to the cueing algorithm is coarser and only a single polarization is available; the targets of interest may also be different. The target detection rate for the ADTS data for a single polarization was about 0.7 with a false alarm rate of about 10 per square kilometer for one-foot resolution; the detection performance for two-foot resolution was nearly identical, but the discrimination utility at two-foot resolution was drastically reduced compared with one-foot resolution. For the four-foot MASR resolution, the false alarm rate is unlikely to increase drastically; consequently, it is expected to be well below the 100 false alarms per square kilometer assumed for sizing the MASR fine resolution

---

1. Stuart R. De Graaf, "Polarimetric Detection and Discrimination Results at Ka-Band (U)," Record of the 38th Annual Tri-Service Radar Symposium, Fort Monmouth, NJ, September, 1992.

processor. The processing load of the cueing sensor is estimated not to exceed the load required to form a single coarse resolution image.

Figure 3.8c presents a block diagram of the target cueing and fine resolution processor; there will be one fine resolution processor for each detection from the cueing algorithm. The fine resolution processor extracts a 32 x 32 pixel chip, centered on the area identified by the target cueing algorithm, from each of the 16 low resolution images. Each of these chips is FFT'd in the range direction, is corner turned, and is FFT'd in azimuth to return the data to the phase history (PH) domain. A 32-point FFT is used in both range and azimuth for both point designs. The 16 PHs are then reordered in memory to form a single contiguous phase history, effectively improving the resolution by four times in both range and azimuth. By using only the center 22 x 22 samples from each PH, a single 88 x 88 sample phase history is constructed. This new PH is then embedded in a 128 x 128 pixel array of zeroes, is FFT'd in range, and is corner turned in memory. The PGA autofocus algorithm is reapplied to the fine resolution data, and the data is FFT'd in azimuth. The final fine resolution target chip has 128 x 128 pixels and about 1.5 samples per resolution cell; a target identification algorithm is then applied to each of the fine resolution chips.

3.3.4 Size and Weight Estimates

The size and weight estimates of the MASR point designs are shown in Figure 3.12. This estimates assume a single channel system for MASR Point Design 1 and a two channel system for MASR Point Design 2. Figure 3.13 shows the block diagram of the MASR hardware. The following sections describe the major system components.

3.3.4.1 The Waveform Generator (WFG)

The WFG generates the wideband waveform transmitted by the radar to obtain fine range resolution. In the MASR system, the transmitted waveform is a wide band, linear FM chirp. The state-of-the-art in WFG technology is direct digitally synthesized (DDS) waveforms converted to analog signals by means of a digital-to-analog converter (DAC).

For the two points designs, the required RF bandwidth of 600 MHz is transmitted as ten separate pulses of 60 MHz each. Traditional designs require the entire bandwidth to be transmitted in a single pulse. The transmission of the full bandwidth in a single pulse would require a DDS WFG with a DAC clock rate of more than 1.2 GHz, but commercially available DACs have a maximum conversion rate of approximately 800 MHz. Therefore, less than 400 MHz of bandwidth is available with direct pulse generation. To achieve the required bandwidth in a single pulse requires the use of RF frequency multipliers. However, the quanitization noise relative to the carrier will increase by $2\log10$ of the multiplication ratio (6 dB for each frequency doubling). Hence, the breaking up of the required bandwidth into smaller steps is a major plus for the MASR architecture because of the reduced quantization noise.

Sciteq, Inc. sells an all digital chirp synthesizer module (DCP-1A) which can support DAC clock rates up to 500 MHz which provide roughly 230 MHz of available bandwidth. The unit measures 7.08 in.(W) x 5 in.(D) x 1.125 in.(H), weighs approximately 3 pounds (2 pounds is the packaging), and dissipates 16 W. The unit has a frequency resolution of 29.8023 Hz and a typical spurious response of -45 dBc. A newer version of the DCP-1A, the ADS-632, uses an innovative GaAs DAC to achieve -60 dBc worst case spurious response when the synthesized bandwidth is limited to 120 MHz. This commercially available unit can meet the bandwidth and spectral purity requirements of the MASR point designs.

Figure 3.12. Comparison Worksheet For MASR

|	Item	MASR-1 Volume Cu.Ft.	Weight Lb.	DC Power Watts	Item	MASR-2 Volume Cu.Ft.	Weight lb.	DC Power Watts
Front End Assembly								
	Power Amp	0.005	0.75	80	Power Amp	0.005	0.75	80
	Tx Ant.	0.028	0.5	5	Tx Ant.	0.028	0.5	5
	Rx Ant.	0.222	4	40	Rx Ant.	0.222	4	40
	LNA	0.010	1.5	24	LNA	0.021	3	48
	BFN	0.042	3	5	BFN	0.042	3	5
IF Receiver								
	IF & D/A	0.094	5.6	120	IF & DS/A	0.188	11.2	240
	WFG	0.012	0.7	20	WFG	0.024	1.4	40
Controller								
	CPU	0.035	4.5	100	CPU	0.071	9	200
	I/O	0.024	3	75	I/O	0.047	6	150
	ROM/RAM	0.035	2.1	6.75	ROM/RAM	0.071	4.2	17.7
Signal Processing								
	Preproc	0.0029	0.175	6.25	Preproc	0.0059	0.35	12.5
	Pol Form	0.0029	0.175	6.25	Pol Form	0.0059	0.35	12.5
	RFFT	0.0029	0.175	8.75	RFFT	0.0059	0.35	17.5
	CTM	0.0059	0.35	2.2	CTM	0.0118	0.7	4.4
	AZFFT	0.0029	0.175	8.75	AZFFT	0.0059	0.35	17.5
	Image Mem	0.0059	0.35	1.1	Image Mem	0.0118	0.7	2.2
Electronics Total		0.53	27.05	509.05		0.76	45.85	892.3
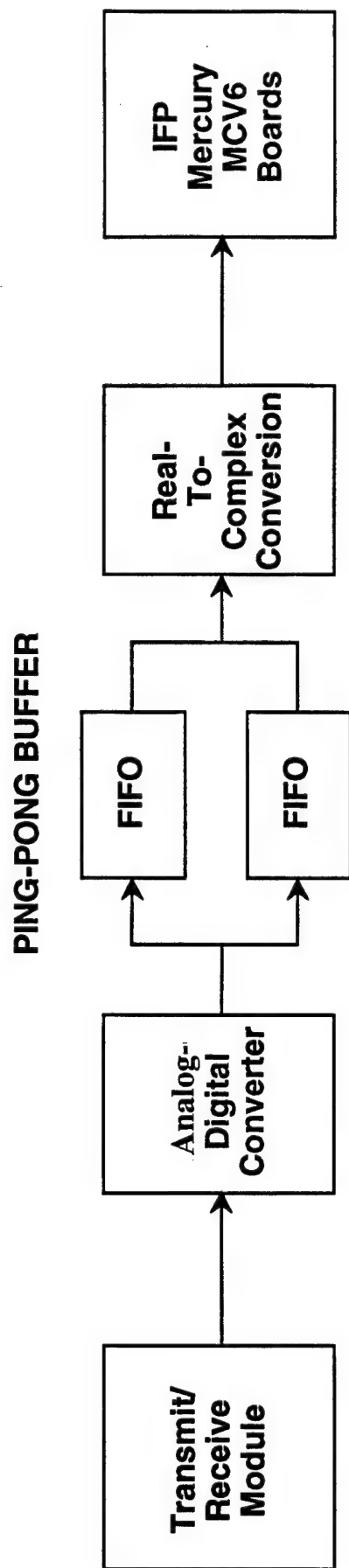
Figure 3.13. MASR H/W Block Diagram

3.3.4.2 Transmit-Receive (TR) Modules

The TR modules used for the MASR point designs in this study are from Texas Instruments (TI). TI manufactures an X-Band TR module which was developed for the MANTECH program. The module, which is solid state and air cooled, delivers 10 W of peak transmitted power and has a 2.5 dB noise figure receiver. The measurements for the module are 7 in x 4.5 in x 1.8 in, and the module weighs 1 lb. and dissipates 23 W. Of the one pound of weight, only 8 oz. belongs to the transmitter and receiver. The other 8 oz. belong to the heat sink, bandpass filter, and power regulator.

Since the MASR center frequency is 15 GHz, this X-band module would not be directly applicable, but TI has also developed a dual-band TR module for the Advanced Shared Aperture Phased Array Radar for the US Navy. This dual-band module operates at X and Ku-bands and can transmit 4 W of peak power. The receiver noise figure ranges from 5.7 to 6.5 dB due to dual band operation. Each TR module weighs 5.3 lbs and dissipates 16.5 W at 33% transmit duty cycle and 66% receive duty cycle. The module dimensions are 4.5 in(W) x 1.65 in(H) x 5 in(D). Currently, a single package contains two TR modules.

As a point of comparison, Westinghouse has a TR module covering the 15-17 GHz band with a maximum transmitter power of 3 W. This module is 18% efficient with transmission bandwidths up to 1 GHz. These TR modules are packaged in groups of four with dimensions of 0.2 in(H) x 0.4 in(W) x 4 in(D).

3.3.4.3 A/D Converter (ADC), Buffer and Preprocessor

The baseband video from each receiver channel is sent to an A/D Converter and Buffer module in preparation for processing. The video signal is digitized at a relatively low 12 or 30 MHz clock rate into 8-bit digital samples. The digitized video is then rate buffered to reduce the instantaneous data rate. A ping-pong buffering scheme is used to accomplish the data rate slow down, as well as to allow for the pipelining of the data processing. As one radar return is being digitized and stored in one memory bank, the previous pulse collected is being read out of another memory bank into the preprocessor at a slower average data rate.

For the MASR point design, an A/D converter from Analog Devices (the AD9000) was selected. This IC consumes approximately 675 mW of power; support circuitry for the ADC consumes roughly 500 mW of power. Two FIFOs are used to create the two memory banks of the ping-pong buffer.

The preprocessor converts the data from a real representation to a complex representation. The conversion is accomplished by modulating the data with a complex exponential. This moves the positive frequency side band down to DC. Low pass filtering is then applied to remove the negative frequency sideband from the frequency spectrum of the signal. Finally, the data is modulated by a complex exponential again to move the remaining sideband back to its appropriate frequency band. In this way, the real radar returns are converted to a complex representation.

The low pass filter used for the real-to-complex conversion is based on a 33 point FIR filter designed with the proper half-band frequency response. The implementation of the filter could be simplified, however, because almost all of the odd filter values are zero. Setting all of these near zero values to zero greatly reduced the hardware necessary for the filter while still maintaining a good frequency response. The real-to-complex conversion circuitry for the MASR point design consists of 3 Xilinx 4010 Field Programmable Gate Arrays (FPGAs), 6 PROMs (look-up tables), and a small amount of support circuitry.

30

Each ADC/Buffer/Preprocessor channel is projected to consume roughly 9 W of power. MASR Point Design 1 requires 1 of these channels, while MASR Point Design 2 requires 2 channels.

3.3.4.4 The Image Formation Processor (IFP)

The real-time image formation processor algorithm is hosted on COTS hardware supplied by Mercury Computers, Inc. The MCV6 processing boards use Intel I860 RISC processors in a multi-processing architecture. Each MCV6 board (6U VME format) can accept up to two daughter cards, each of which can hold two compute elements (CEs). Each CE contains one I860 processor, up to 4 Mbytes of memory, and a crossbar ASIC for the Mercury Raceway multiprocessor interconnect bus. See Figure 3.14. Therefore, each MCV6 board can contain 4 I860s and up to 16 Mbytes of memory.

The Mercury Raceway bus is an important part of the IFP architecture. It allows for high speed interconnections between the processors. Each crossbar ASIC provides four non-blocking connections at 160 Mbytes/sec. See Figure 3.15.

The MCV6 board conforms to the 6U VMEbus standard. It measures 6inx 9in x 0.8in, draws less than 28 Watts of power, and has a standard VMEbus interface on the P1/P2 connectors. A diagram of the MCV6 board is shown in Figure 3.16. The P2 connector is also used to propagate the Raceway bus from board to board. See Figure 3.17 for a diagram of a four board interconnection with the Raceway interlink.

The operations performed by the IFP include motion compensation, two-dimensional interpolation (polar formatting), fast-fourier transforms (FFTs), and corner turns. These operations were mapped to the Mercury hardware by means of benchmarking information on the various operations the board could perform. For example, Motion Compensation consists of generating a complex vector whose frequency and phase are determined by the motion of the platform and then multiplying the received range data pulse with this vector. The vector is specified by its frequency and phase offset. The benchmark for the Mercury subroutine call VXCS (which generates a complex vector of a particular frequency and phase) is 170 nanosec/point. The complex multiply operation is benchmarked at 110 nanosec/point when operating out of cache. Therefore, the total time for motion compensation can be benchmarked at 280 nanosec per input point.

Similarly, benchmarks are available for the other image formation operations that must be performed. See Figure 3.18 for FFT benchmarks of the MCV6 board for various FFT lengths N from 7 to 12.

CE
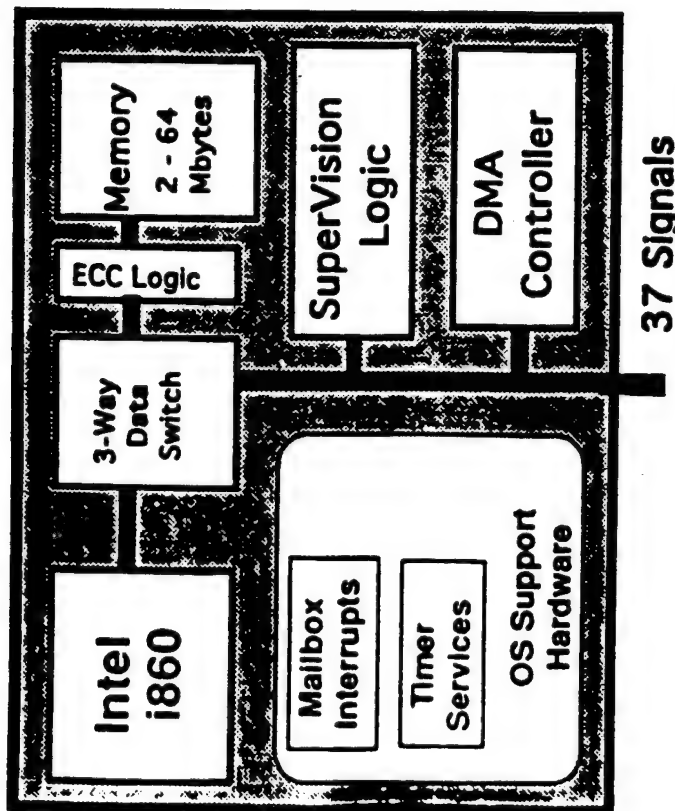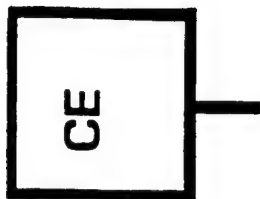
Each CE has:

- Intel i860 XR 40Mhz
- Three Way Data Switch
- DMA Controller
- ECC Memory
  - Corrects Single Bit Errors
  - Detects Double Bit Errors
- SuperVision Logic
  - Monitors Traffic
  - Non-Intrusive
- All CE Logic in Single ASIC
- MC/OS Software

Memory
2 - 64
Mbytes

ECC Logic

SuperVision
Logic

DMA
Controller

3-Way
Data
Switch

Intel
i860

Mailbox
Interrupts

Timer
Services

OS Support
Hardware

37 Signals

to cross bar

Figure 3.14. Mercury Compute Environment (CE)

XBAR

XBAR

CE0 CE1 CE2 CE3
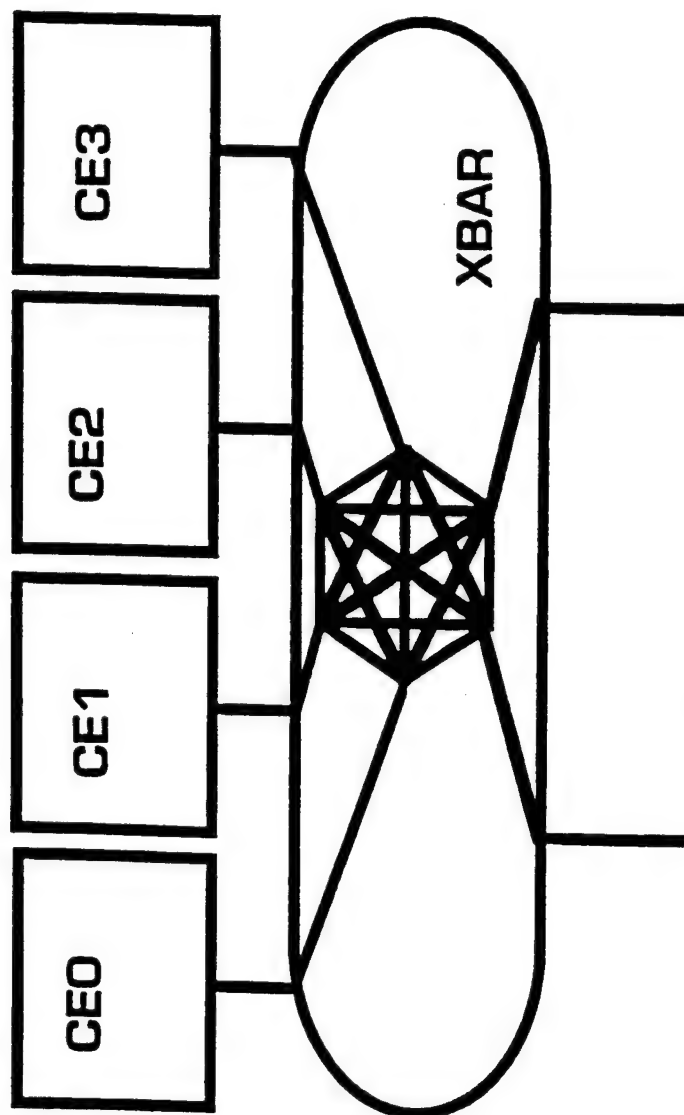
- **Single ASIC Device**
- **6 Ports (160 Mbytes/Sec/Port)**
- **3 Point to Point Connections (480 Mbytes/Sec)**
- **1-> 5 Port Broadcast (800 Mbytes/sec)**

MERCURY
Computer Systems Inc

Figure 3.15. RACEway Cross Bar ASIC

Figure 3.16. MCV Circuit Card
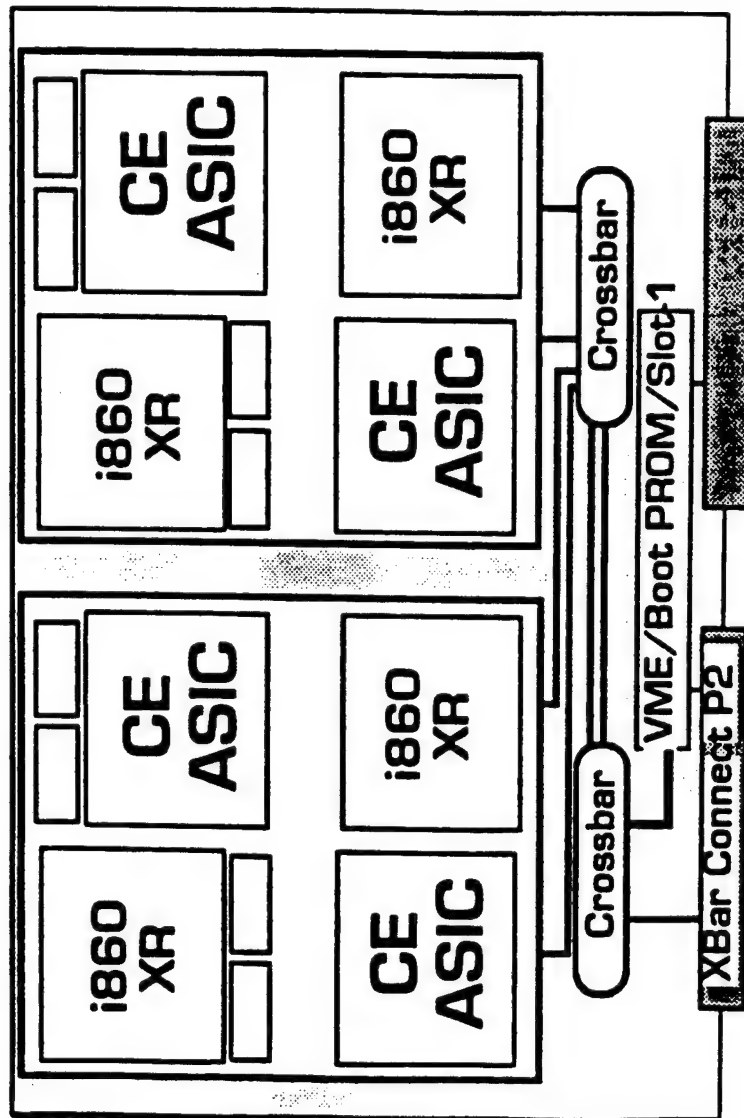
- Two daughtercards
- Boot PROM with optional Slot-1
- Typical power consumption <25w

34
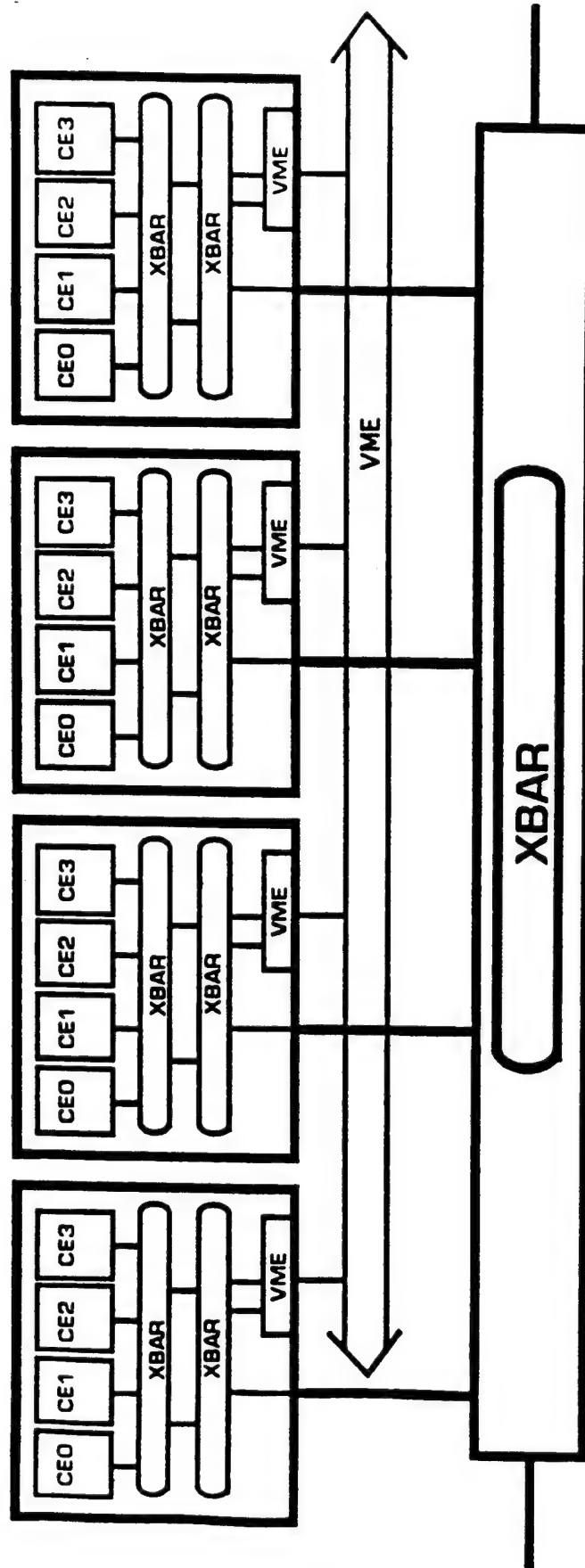
Figure 3.17. RACEway Interlink

N	Length	Butterflies	Bench Mark	Butterflies/pixel	Butterfly Time	MPixels/sec
			μs		ns	
7	128	448	67	3.5	150	1.91
8	256	1024	150	4	146	1.71
9	512	2304	330	4.5	143	1.55
10	1024	5120	740	5	145	1.38
11	2048	11264	2030	5.5	180	1.01
12	4096	24576	4300	6	175	0.95

Figure 3.18. FFT Benchmarks—MCV6 Board

4.0 MASR/SAR-P COMPARATIVE STUDY

Although any SAR system contains the same components, the MASR system approach results in different requirements for many components. In comparing the SAR-P and MASR architectures, the affected components are the antenna, the transmitter, the waveform generator, the A/D buffer, the waveform generator, and the processor. The IF receivers happen to be similar, but the output data formats are different. The SAR-P system uses a receiver with inphase and quadrature (I &Q) channels, while the MASR system uses one offset video channel whose output is converted to I and Q video in the processor. The receiver formats do not significantly affect the remainder of the components such as the motion compensation system, the controller, and the timing generator. Section 3 has a detailed description of the MASR system, and Section 4.2 has a brief description of the SAR-P system.

4.1 COMPARISON METHODOLOGY

The objective of this study is to compare the pros and cons of the SAR-P system and MASR Point Design 1. The basis for comparison will include the floating point operations per pixel, and the pixels rates per unit volume, weight, and power. For MASR Point Design 1, the relationship between the total number of operations needed per image versus the number of fine resolution target chips generated is quantified.

4.2 SAR-P SYSTEM DESCRIPTION

The Sandia National Laboratories has developed the SAR-P and flown the system in a Twin-Otter Testbed. The radar collects data in both stripmap and spotlight modes with variable squint and depression angles; the SAR-P has real-time onboard processing and real-time GPS-aided navigation with accurate position (< 5 m) and accurate velocity measurement (<0.1 m/s). Table 4.1 lists some of the key SAR-P parameters; the SAR-P uses direct digital synthesis technology for the transmitted waveform. The SAR-P, which operates at a center frequency of 15 GHz, is designed for short range operation from a slow moving, unmanned aerial vehicle (UAV). Figure 4.1 is a simplified block diagram of the SAR-P, and Figure 4.2 is a radar signal-flow diagram.

The real-time processor features a large swath, which is 1800 pixels wide, and continuous coverage at a velocity of 70 m/s. The stripmap resolution is greater than or equal to P, and the spotlight resolution is greater than or equal to P/2. Important motion compensation operations are performed before the digitization of the return signal. Spatially variant, high-order focus is provided in a dynamic environment. There is compensation for motion through resolution cells with an overlapped subaperture algorithm and phase rotation. The signal processor utilizes efficient FFT processing techniques, vector multiplication, and real-time phase gradient autofocus (PGA). Figure 4.3 shows the signal-processor data flow, and Figure 4.4 is a block diagram of the Sandia processing algorithm.
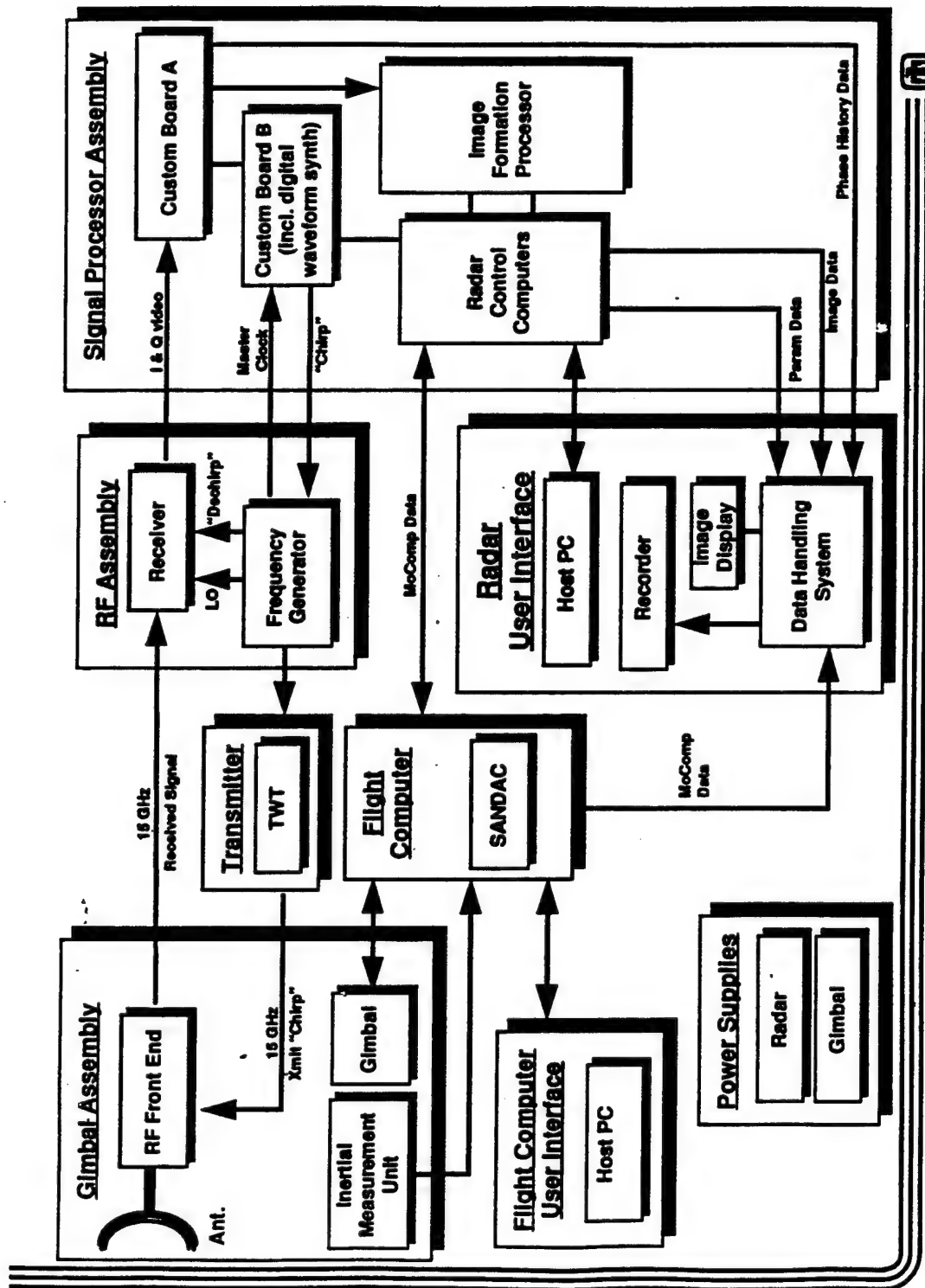
Figure 4.1. Existing SAR-P Sensor Block Diagram
(From Sandia Briefing)
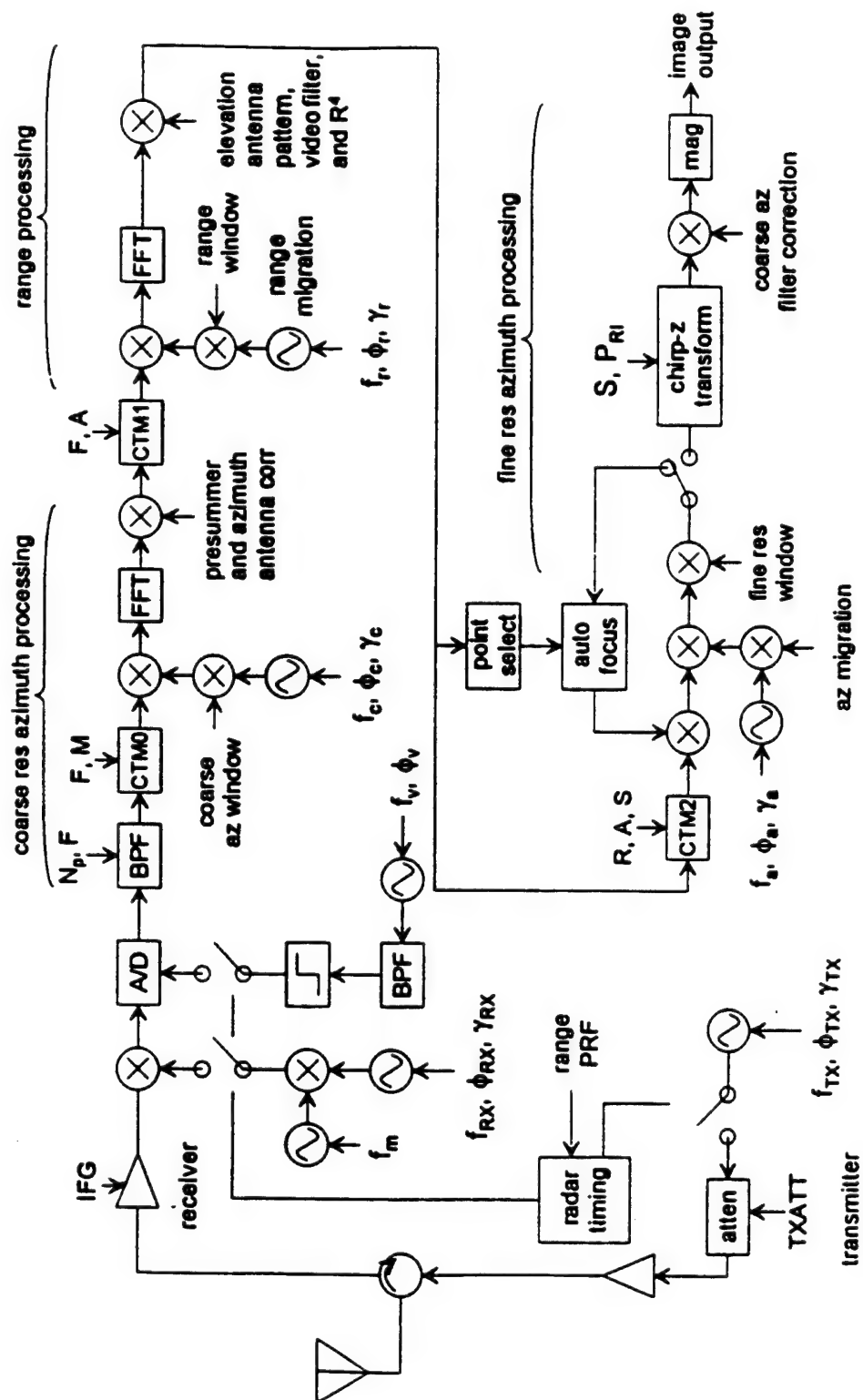
Figure 4.2. SAR-P Radar Signal Flow Diagram
(From Sandia Briefing)
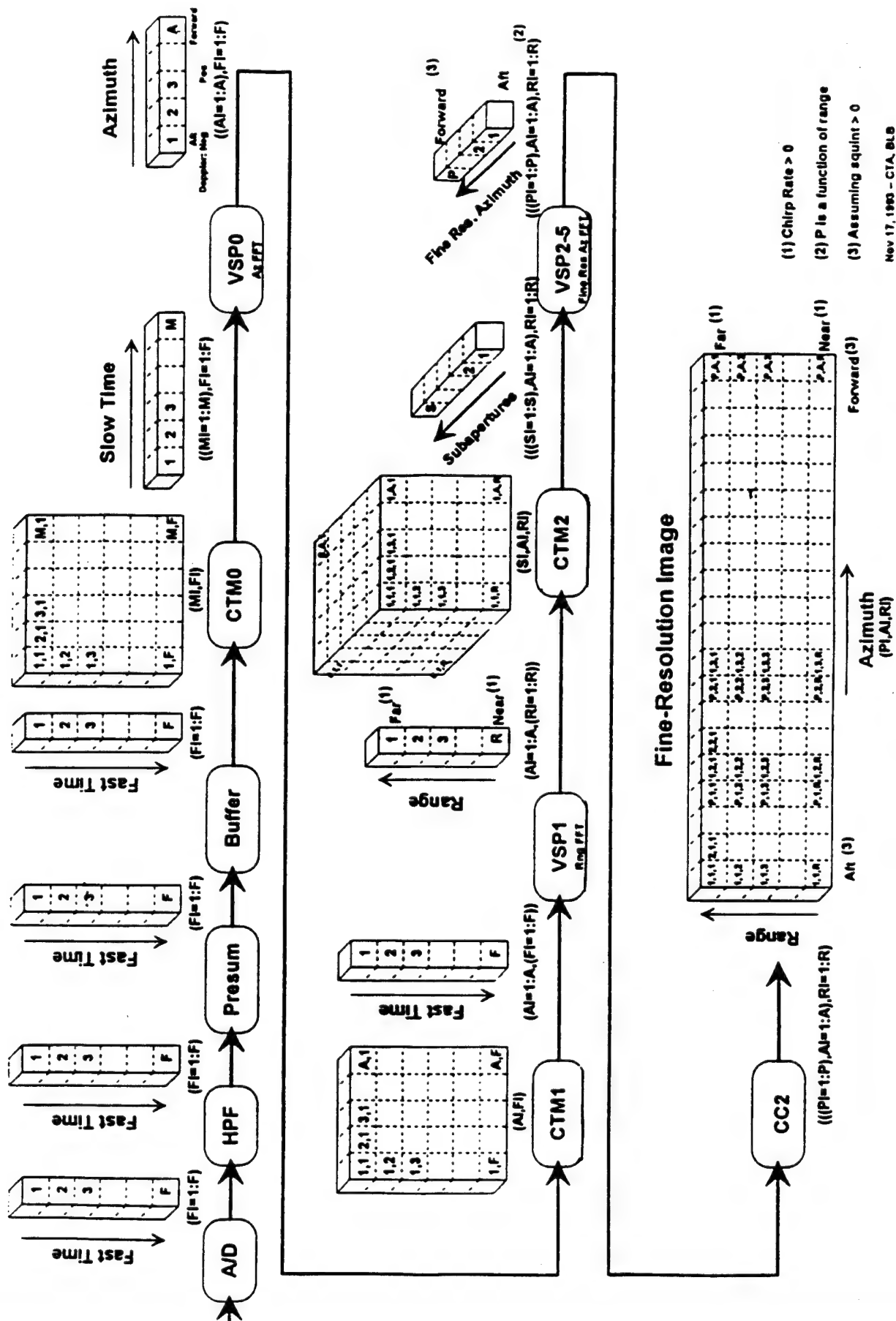
Figure 4.3. SAR-P Signal Processor Data Flow Diagram

Figure 4.4. Sandia SAR-P Processing Algorithm Block Diagram

NSR = # of Subapertures in Range
NSA = # of Subapertures in Azimuth
SASA = Subaperture Size in Azimuth
SASR = Subaperture Size in Range
AZKEEP = # of Samples to Keep After Coarse Azimuth Processing
SASR2 = Subaperture Size in Range for Range Process
RNGKEEP = # of Samples to Keep After Range Process
NIR = # of Image Samples in Range
NIA = # of Image Samples in Azimuth

41

Table 4.1. Some Key SAR-P Parameters

Parameter	Value
SAR Modes	Strip Map Spotlight
Strip Map Resolution	P to 10 P Meters
Spotlight Resolution	0.5 P to 10 P Meters
Center Frequency	15.0 GHz
Swath Width	1800 pixels
Range	4 - 8 km
Grazing Angle	15 to 90 degrees
Squint Angle	45 to 135 degrees
Dynamic Range	> 75 dB
Additive Noise	< -25 dB
MNR	< -10 dB
Peak Trans. Power	30 W
Noise Figure	1.5 dB
A/D Resolution	8 bits
A/D Sample Rate	67 MHz
Sample Method	I and Q

4.3 SYSTEM COMPARISON

The SAR-P and MASR systems were compared using operations per pixel and pixels per unit weight, volume, and power. The next sections describe these comparisons in detail and present the final results.

4.3.1 Operations Per Pixel

An operations/pixel comparison was made between the SAR-P and the MASR algorithms. An estimate of total operations was generated by counting the total number of complex operations performed at each major algorithmic step. A complex operation is defined as one radix 2 FFT butterfly. A single FFT butterfly consists of one complex multiply and two complex additions. This further equates to four floating point multiplies and six floating point additions, or a total of ten floating point (real) operations. We used this 10-to-1 complex to real operation conversion at all stages of evaluation, not just for the FFTs. This admittedly exaggerates the operations counts for

non-FFT steps. It does, however, compensate the overall estimate by providing a margin for uncounted machine cycles such as array index generation and memory access.

Flow diagrams were sketched for the SAR-P and MASR algorithms. Key numerical operations—such as a complex multiply or FFT—were identified at each key step. Data sizes were computed and were given a label. General equations expressing the total complex operations occurring at each algorithmic step were then written. For convenience, all parameters and equations were placed in a spread sheet and the results were compiled (see Tables 4.2 and 4.3). The same output image size was used for the two algorithms, and both algorithms employed PGA as an autofocus approach.

Table 4.2. SAR-P Algorithm

System/Processing Parameters	
Samples per Pulse	1638
Pulses per Subaperture	64
No. of Range Subapertures	1
No. of Azimuth Subapertures	150
Range Samples to Keep	1800
Azimuth Records to Keep	25
Range Batch Size	2048
Fine Azimuth Batch Size	256
Range Image Pixels	1800
Azimuth Image Pixels	1650
Total Image Pixels	2970000
Complex Operations Count/Scene (in Millions)	
Range Processing	57.6
Fine Azimuth Processing	225.3
Total Complex Operations	361.6
Total Operations	3,616

Table 4.3. MASR Algorithm

System/Processing Parameters	Design 1	Design 2
Complex Samples per Pulse	1715	6810
Pulses per Aperture	2640	2640
Range Phase Histories	1670	6670
Azimuth Phase History Size	1270	1270
No. Range Subapertures	4	4
No. Azimuth Subapertures	4	4
Range Subaperture Size	512	2048
Azimuth Subaperture Size	512	512
Range Subimage Size	32	32
Azimuth Subimage Size	32	32
Polar Interp Filter Length	10	10
Range Image Pixels	1800	
Azimuth Image Pixels	1650	
Coarse Processing Complex Operations Count/Scene in Millions		
Motion Compensation	22.6	89.9
Presumming	104.1	413.5
Range Polar Interpolation	22.0	88.0
Azimuth Polar Interpolation	33.5	33.5
2-D FFT of the 16 Subapertures	37.8	167.8
Fine Processing Complex Operations Count (100 detections/km^2) in Millions		
Alarms per Patch	19	79
2-D FFT of All Coarse Resolution Chips	1.9	7.7

Table 4.3. MASR Algorithm (Continued)

System/Processing Parameters	Design 1	Design 2
2-D FFT of All Fine Resolution PHs	2.2	9.1
PGA Autofocus of All Fine Res Chips	1.6	6.8
Total Complex Operations	225.8	816.3
Total Operations	2,258	8163

Figure 4.5 shows a graphical comparison of the operations counts for the SAR-P and the MASR image formation algorithms. Each is plotted against the number of target detections per image. As an additional comparison, we have added the operations count for conventional polar format processing. The curves for SAR-P and the polar format algorithms are flat with the number of target detections because they always form the entire image. The MASR algorithm forms one fine resolution image chip for each target detection; hence, its computational load increases with the number of detections. The maximum number of detections considered in this analysis was 275. At this point, the total area mapped by the MASR fine resolution image chips equals the total area of a single MASR frame.
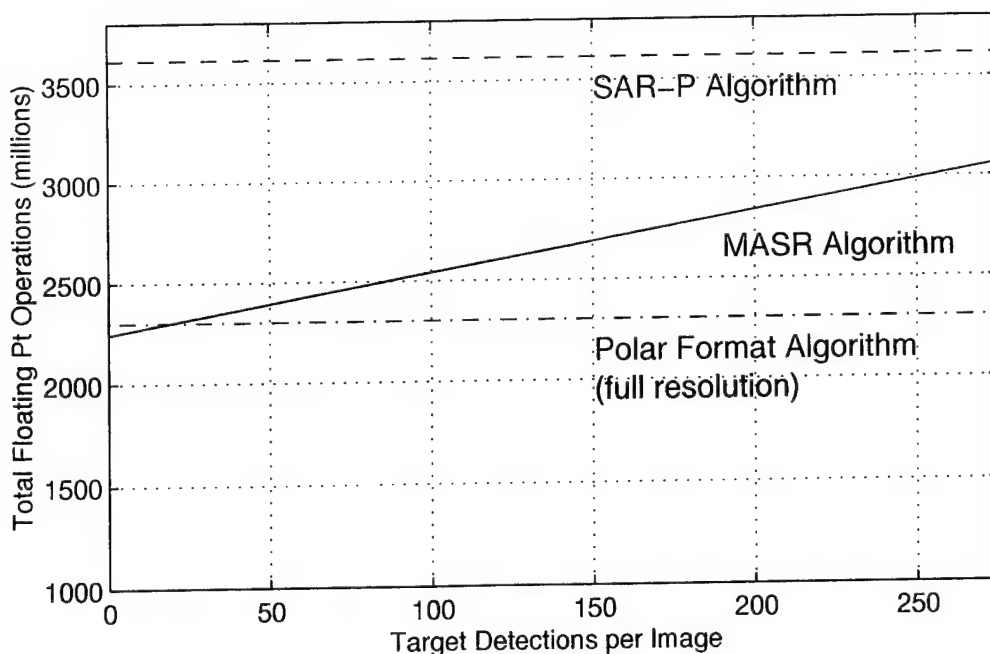
Figure 4.5 Floating Point Operations Versus Target Detections Per Image

The curves indicate that most of the computational advantage of the MASR algorithm can be attributed to its basis in the polar format algorithm. The specific MASR changes provide only a 2% to 6% improvement over conventional polar formatting, and then only for a small number, approximately 30, of detected targets. This small improvement is not significant enough to warrant the use of the MASR algorithm for image formation.

4.3.2 MASR Hardware Reductions from SAR-P

The MASR Point Design 1 architecture results in modest reductions in the size, weight, and power of the overall radar system. In the transmitter, there is a reduction in size and weight, but not in the prime power because the average power transmitted is assumed to remain constant. With the sensor digital components, the only significant saving is in the prime power; however, with the processor, there are savings in the size, weight, and prime power.

The SAR-P solid-state transmitter provides a peak power of 30 watts; it weights 9 pounds with cooling, and its volume is 73.5 cubic inches. A 10 watt peak power T/R module for the MASR transmitter is estimated to weigh 1 pound and have a volume of 16 cubic inches. For a typical SAR system such as the ERIM IFSARE, the transmitter is approximately 7.5% of the total system weight and volume. The system wide weight savings using the MASR Point 1 design will, therefore, be 8/9ths of 7.5% or 6.7%; the system wide volume savings will be (57.5/73.5) of 7.5% or 5.9%.

There will be a prime power savings for the sensor's front end digital circuitry, but no savings in weight or volume. The reduced peak data rates at the radar front end will allow the use of CMOS ICs instead of ECL ICs; consequently, the A/D converter, the data buffer, and the digital waveform generator will experience a power saving because of the much lower power consumption of CMOS circuitry. The estimated savings in prime power is 75%; however, these circuits are estimated to use only about 3.5% of the total system prime power. The system wide power savings

46

will, therefore, be limited to 0.75 times 3.5% which equals 2.6%. Since the buffer evens out the data rate, there will be no power savings for the digital circuits after the buffer.

The size, weight, and power consumption of the processor can be assumed to be proportional to the number of processor operations per scene. Since the MASR 1 processor with the polar format algorithm uses 2.26 Gflops compared with 3.62 Gflops for the SAR-P, there is a 38% saving. Assuming that the processor accounts for 25% of the size, weight, and power of, the system, the MASR1 system savings will be 0.38 time 25% or 9.5%.

Table 4.4 summarizes the estimated MASR1 hardware savings over the SAR-P. The savings for the overall SAR system are 16.2% in weight, 15.4% in volume, and 12.1% in prime power.

Table 4.4 Estimated MASR/SAR-P Hardware Savings

Factor	Transmitter	Digital Sensor Hardware	Processor	Total Overall System Savings
Weight	6.7%	-	9.5%	16.2%
Volume	5.9%	-	9.5%	15.4%
Power	-	2.6%	9.5%	12.1%

4.3.3 Pixel Rate Per Unit Volume, Weight, and Power

The pixel rate for the SAR-P in the stripmap mode equals the product of the swath width in pixels, 1800, and the pixel rate in azimuth. Assuming 1.5 pixels/IPR, the azimuth pixel rate will be 1.5 times the velocity divided by the resolution. The total number of pixels/ sec is 6.2×10^5. For the MASR1 design, it will be assumed that the pixel rate equals the number of fine-resolution pixels in the area searched, not the number of pixels in the fine-resolution chips. The number of pixels in the fine-resolution chips would be too small for a meaningful comparison when there are few detections. Assuming the same platform velocity for both systems, the area search rate will be the same. The pixel rates shown in Table 4.5 are thus equivalent to the overall system savings in weight, volume, and power.

Table 4.5 MASR Pixel Rate Improvement

Quantity	MASR Improvement Over SAR-P
Pixels/sec/unit weight	16.2%
Pixels/sec/unit volume	15.4%
Pixels/sec/watt	12.1%

4.4 TARGET CHIP DENSITY FOR MASR DESIGN

One can estimate the percentage of the scene that can be processed in fine resolution using the same processing resources that were used in the coarse resolution cycle. In the coarse resolution cycle, the required 2-D FFTs are performed on 16 looks during one fine resolution aperture time. The FFT sizes are 512x512 for the 0.5 km case and 1024x512 for the 2 km case. The corresponding number of 128x128 fine resolution FFTs is 256 and 512; respectively. Each fine resolution segment required a 32x32 point 2-D inverse FFT to be performed on each of the sixteen looks. It also requires a 128x128 point 2-D FFT to be performed on each of the 256 segments. The ratio of the time available to do the fine resolution transformation to that of the coarse resolution is 0.22 for the 0.5 km case and 0.12 for the 2 km case for the polar format processing resources now available for FFT in both cases. The end result is approximately 48.2% of the scene can be processed in fine resolution in the 0.5 km example and 19.8% in the 2 km example.

5.0 MASR ALGORITHM VERIFICATION

5.1 VERIFICATION OBJECTIVE

The objective of the verification effort was to validate the performance of the MASR fine resolution image formation algorithm. This was accomplished by demonstrating the algorithm on one and two-dimensional data sets obtained from both simulated and real radar systems. Coarse mode to fine mode resolution improvements of 2:1 and 4:1 were examined.

5.2 IMAGE FORMATION ALGORITHM VERIFICATION APPROACH

The verification approach was to exercise both the MASR and conventional processing algorithms on a set of test cases and then to compare the results. Both one- and two-dimensional implementations of the MASR algorithm were constructed, and each had unique benefits. The one-dimensional simulation was useful in that it was easy to create and process phase histories incorporating various effects such as noise and multiple targets. The two-dimensional simulation produced actual SAR imagery. The imagery is more useful in assessing the utility of the final product, and it allows for the measurement of various image quality parameters such as impulse response widths and signal-to-background ratios.

The one-dimensional simulation was implemented in MATLAB, a commercially-produced interpreted language with built-in support for matrix algebra, signal processing operations, and graphics. The two-dimensional simulation was constructed using a set of ERIM-developed UNIX programs collectively known as IMGMANIP. IMGMANIP programs operate on whole data files and provide a wide assortment of mathematical, signal processing, and display operators. The programs may be chained together into complex processing sequences using the UNIX piping facility and UNIX script files.

5.3 MASR ALGORITHM DESCRIPTION

The MASR algorithm conserves computational resources by limiting fine resolution image formation processing to areas likely to contain targets of interest. Because of this, the MASR algorithm depends heavily upon an advanced target cueing algorithm to identify these target areas. To achieve the computational savings, the cueing algorithm must be applied to coarse resolution image data.

In its implementation, the MASR algorithm overlays the polar format algorithm (PFA) for SAR image formation processing. The three key components of the PFA are motion compensation, polar-to-rectangular interpolation, and a two-dimensional FFT. With MASR, the first two PFA steps are unchanged—the collected SAR data is motion compensated and undergoes a full-resolution polar-to-rectangular interpolation. During polar interpolation, however, the MASR algorithm subdivides the full-resolution, two-dimensional phase history (PH) array into 16 PH chips of equal size. Performing a two-dimensional FFT on any chip produces a reduced resolution image of the illuminated scene. Because the array was divided into four pieces in both range and azimuth, the final image resolution is coarser by a factor of four.

The target cueing algorithm is applied to one of the coarse resolution chips at this point, and it identifies image areas that contain targets of interest. Since most targets are physically small compared to the total coverage area of the image, we only need process the cued image areas to fine resolution. The MASR algorithm computes the fine resolution image chip by appropriately combining portions of the 16 low-resolution images. The combining procedure is as follows. First, a 32 x 32 pixel region, centered on the detected target, is subsetted out of each of the 16 coarse reso-

lution images. Each 32 x 32 region is 2-D inverse FFT'd. The center 22 x 22 region is removed from each of the resulting signal history chips. The 16 chips are next butted up against each other in both range and azimuth in accordance with their original position in the initial polar interpolation array. This operation forms a new signal history that is 88 x 88 samples in both range and azimuth. The 88 x 88 array is embedded into another array of zeroes that is 128 x 128 samples and then is 2D FFT'd. This forms a fine resolution image of the cued target area with about 1.5 samples per resolution cell. The PGA autofocus algorithm is again applied to the image to removed any residual image misfocus. The image is then detected and passed to the image display or image interpreter.

5.4 ONE-DIMENSIONAL SIMULATIONS

The one-dimensional MATLAB software simulates a single received pulse containing three scatterers. No noise was added to the signal data, although the simulator supports such a choice. This 1D MASR algorithm implemented a 4:1 resolution improvement.
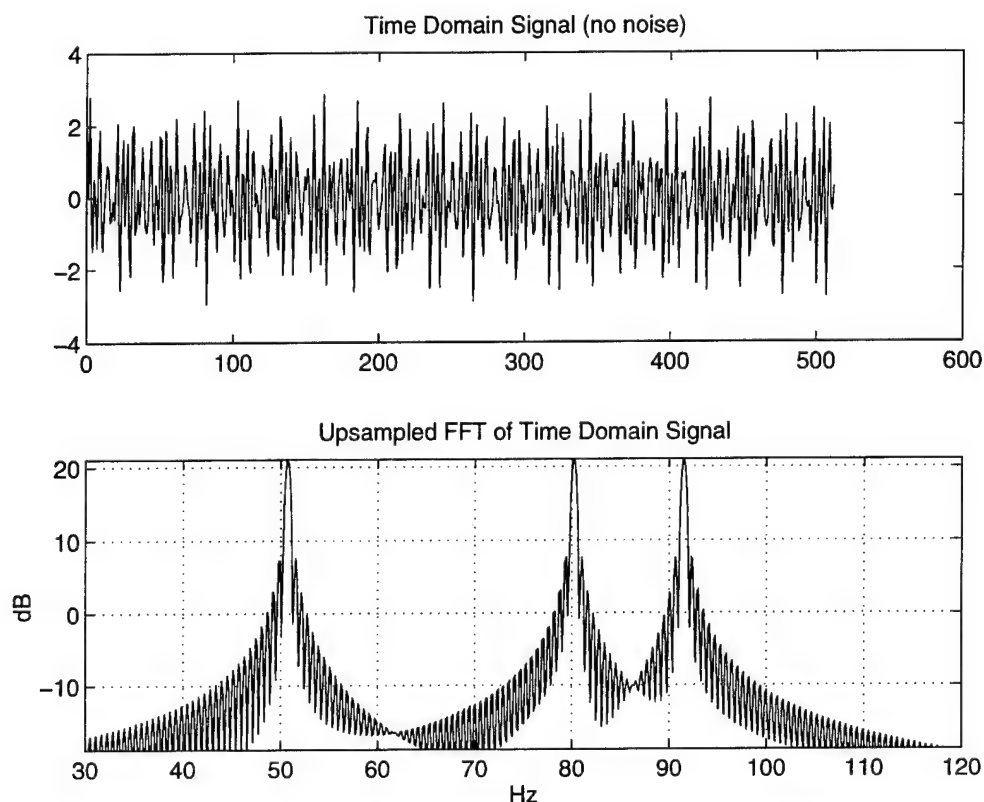
Figure 5.1. Simulated Time-Domain Signal (Upper) and Its Upsampled FFT (Lower)

The upper graph in Figure 5.1 shows the noiseless time-domain signal for three point targets; 512 samples were generated. The lower graph presents the upsampled FFT of the time-domain signal.

50

The upper graph in Figure 5.2 presents the non-upsampled FFT of the time-domain signal of Figure 5.1. This graph is representative of the results that one would obtain via conventional polar format image formation processing. The lower graph in Figure 5.2 depicts the results of MASR processing of the 1D image. Please note that the point target responses occur at the same frequencies in both graphs, so the MASR algorithm introduces no position distortions. Note also that the MASR processing does introduce some elevated sidelobes that are not present in the FFT-processed data. These sidelobes are an unavoidable by-product of the algorithm. No aperture weighting was used in either case.
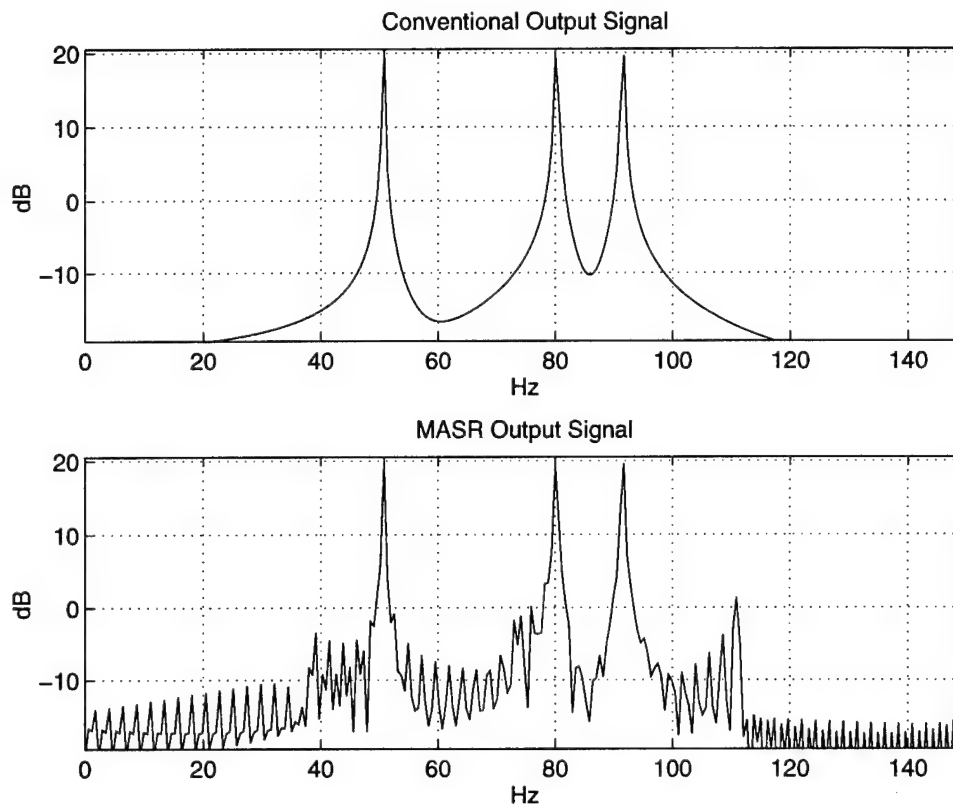

Figure 5.2. FFT-Processed Signal Data (Upper) and MASR-Processed Data (Lower)

As a final example from the one-dimensional simulations, the upper portion of Figure 5.3 again depicts the upsampled FFT of the time-domain signal of Figure 5.1. Again, this represents the results from conventional polar format processing. The lower portion of Figure 5.3 shows upsampled results from MASR processing. Again, the targets appear in their correct spatial positions and some elevated sidelobes have been introduced by the algorithm.

5.5 TWO-DIMENSIONAL SIMULATIONS

The 2-D simulation made use of airborne SAR data from the ERIM DCS and implemented a 2:1 resolution improvement. The chosen image is shown in Figure 5.4, below. The scene is a radar test array installed near Willow Run Airport in Ypsilanti, Michigan. The target area select for
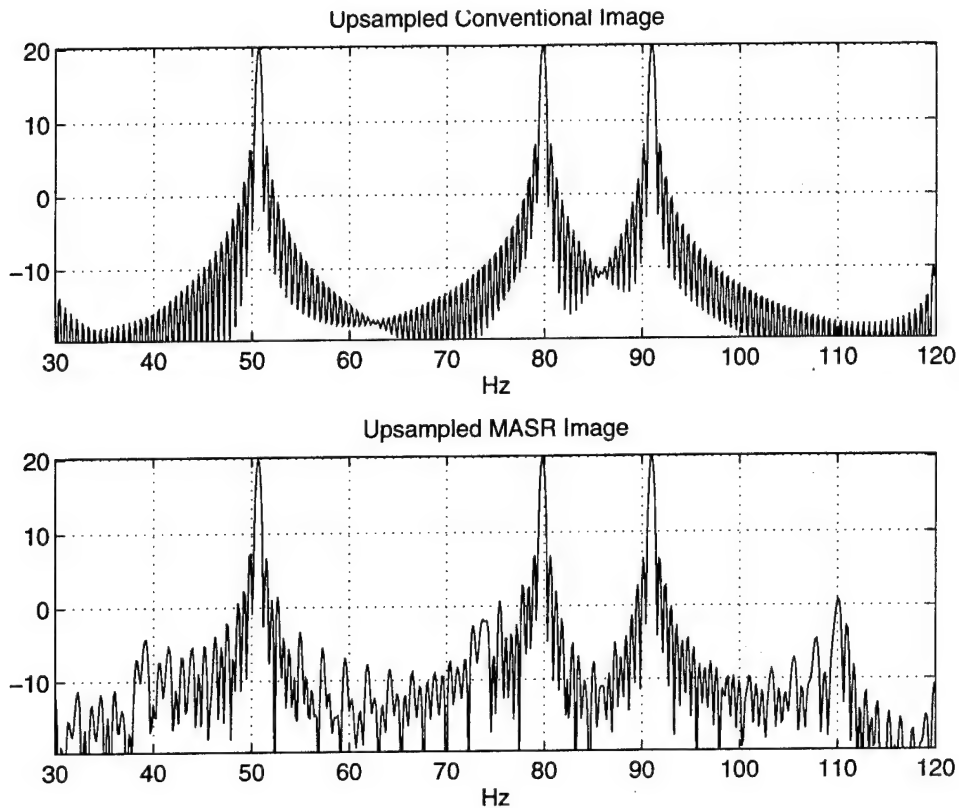
Figure 5.3. Upsampled, FFT-Processed Signal Data (Upper) and MASR-Processed Data (Lower)

MASR processing was centered on the point target just to the left of "A" on the diagram. No aperture weighting was placed on the phase history to control sidelobes in the images.

The radar data collected over the test array was conventionally processed with the PFA to a range and azimuth resolution of 1m. An image quality measurement tool was used to verify the resolution of the conventionally processed image. The interpolated phase history was next divided into four pieces, and each piece was 2-D FFT'd and autofocussed. This produced four images of the scene, each with 2m resolution in both range and azimuth. Following this, 64 x 64 pixel image chips, each centered on the chosen point target, were extracted from the four low resolution images. The image chips were 2-D inverse FFT'd and the resulting phase histories were butted together to form a single phase history with size 128 x 128 samples. The new signal history was 2-D FFT'd. The resulting fine resolution target chip is shown in Figure 5.5.

Range and azimuth impulse response plots were made for the point target in the center of the fine resolution, MASR-processed image chip. The measurements verified that the final image resolution was indeed 1m in both range and azimuth. The impulse response plots are presented in Figure 5.6(a) and (b).
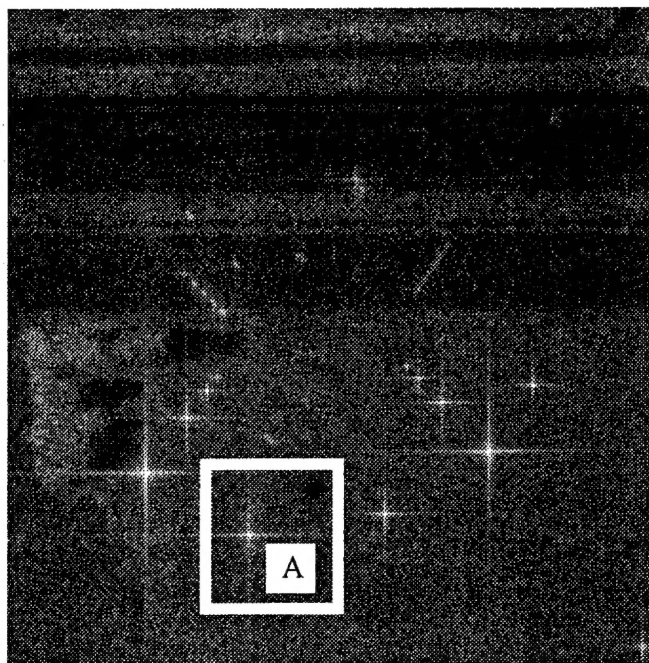
52

Figure 5.4. Full-Resolution, Conventionally Processed Image of the Test Array
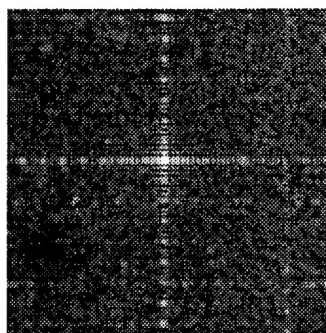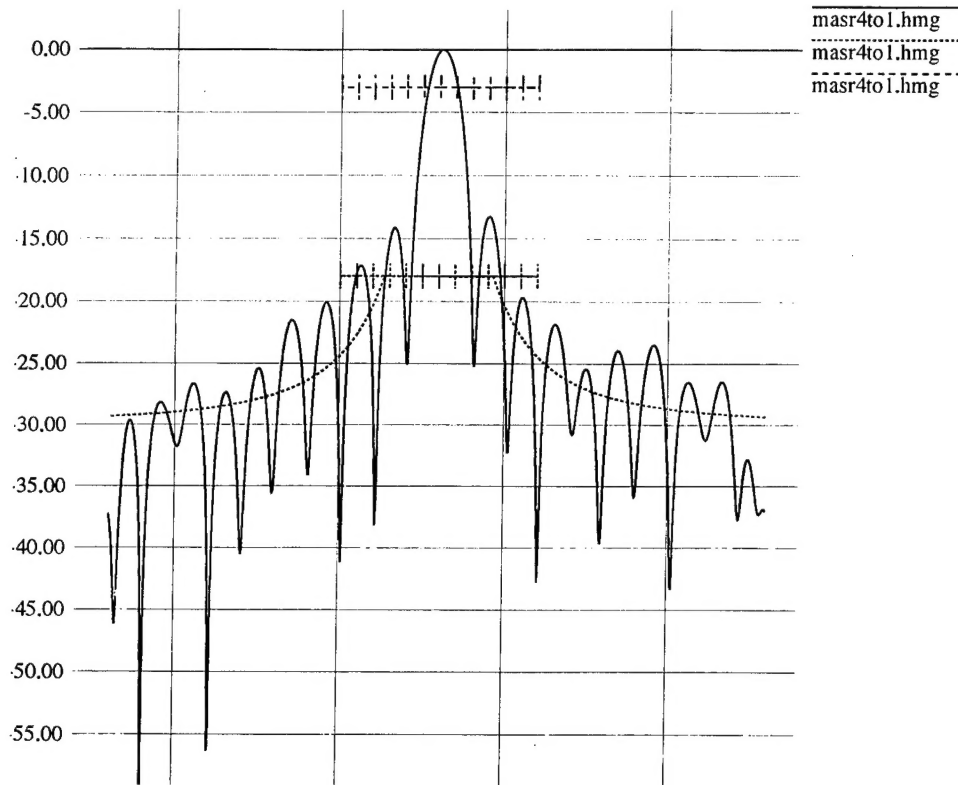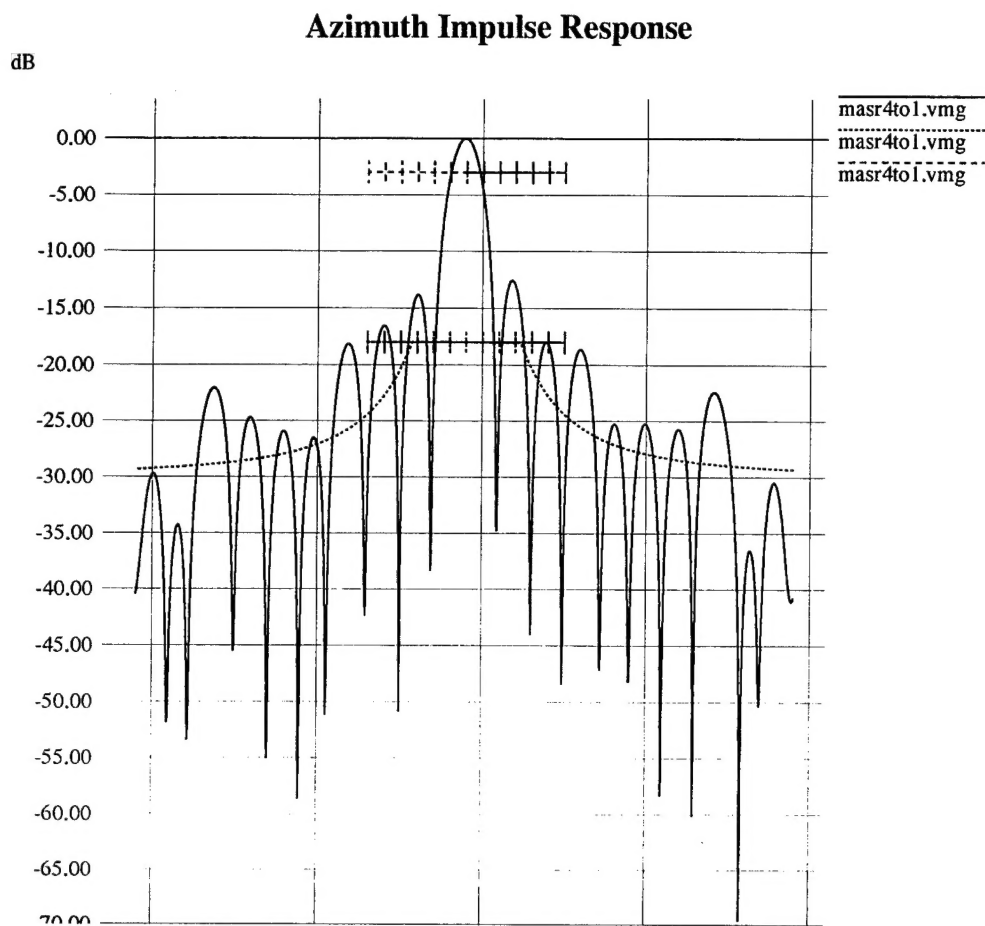

Figure 5.5. Full-Resolution, MASR-Processed Image Chip of the Test Array

Range Impulse Response

(a)

Figure 5.6. **Range (a) and Azimuth (b) Impulse Response Plots From the MASR-Processed Image**

Azimuth Impulse Response

(b)

Figure 5.6. Range (a) and Azimuth (b) Impulse Response Plots From the MASR-Processed Image

6.0 CONCLUSIONS AND RECOMMENDATIONS

6.1 CONCLUSIONS

The MASR approach provides advantages for both the radar hardware and the processor for a system with requirements similar to those of the SAR-P. The split range bandwidth architecture trades fewer samples per pulse for more pulses per second, resulting in the need for lower peak transmitter power. The lower peak transmitter power would have a size and weight advantage but not a prime power advantage, because the average transmitter power must be maintained. Prime power, however, would be saved in some of the front end radar components because of the lower I/O, FM, and sampling rates in the system. The split bandwidth architecture also reduces the bandwidth and noise. The front end weight, volume, and power savings resulting from the split bandwidth is about 5%. The disadvantage of transmitting more pulses per second is that range ambiguities limit vehicle velocity more than for a low PRF system.

The advantages of polar format image processing over SAR-P processing are significant. There are approximately 37% fewer operations required to polar- format process the entire scene at fine resolution with high image quality. The fewer operations allow a 9% reduction in the system-wide weight, volume, and power because of the smaller processor. The pixel rate improvement per unit weight, volume, and power is about 14%. The minor 3% to 6% additional advantage of dual-resolution processing for fewer than 30 target detections per scene is outweighed by the reduction in image quality and the increased number of operations when more than 30 targets are detected in a scene. The far-out sidelobes are about 15 dB higher than the sidelobes with conventional processing, and the background noise increases about 3 dB; both of these effects make target discrimination more difficult. The MASR approach is, therefore, not recommended.

6.2 RECOMMENDATIONS

This study compared the SAR-P architecture with a single MASR point design concept. The hardware benefits of splitting the range bandwidth into pieces, although modest, should be considered in future radar design efforts. The benefits of polar format processing over segmented FFT processing were more significant and deserve additional consideration. In particular, the efficiency of programming the polar format algorithm using state-of-the-art high speed processor architectures should be investigated further. Finally, other processing techniques, such as planar subarray processing, alternate formulations of the overlapped subaperture algorithm, and possibly tomographic back projection, should be investigated to determine if a more attractive image formation algorithm than the polar format algorithm can be developed.